Modification of Long Equatorial Rossby Wave Phase Speeds by Zonal Currents

THEODORE S. DURLAND, ROGER M. SAMELSON, DUDLEY B. CHELTON, AND ROLAND A. DE SZOEKE

College of Oceanic and Atmospheric Sciences, Oregon State University, Corvallis, Oregon

(Manuscript received 17 May 2010, in final form 30 November 2010)

ABSTRACT

Previously unaddressed aspects of how equatorial currents affect long Rossby wave phase speeds are investigated using solutions of the shallow-water equations linearized about quasi-realistic currents. Modification of the background potential vorticity (PV) gradient by curvature in the narrow equatorial currents is shown to play a role comparable to the Doppler shift emphasized by previous authors. The important variables are the meridional projections of mean-current features onto relevant aspects of the wave field. As previously shown, Doppler shifting of long Rossby waves is determined by the projection of the mean currents onto the wave's squared zonal-velocity and pressure fields. PV-gradient modification matters only to the extent that it projects onto the wave field's squared meridional velocity.

Because the zeros of an equatorial wave's meridional velocity are staggered relative to those of the zonal velocity and pressure, and because the meridional scales of the equatorial currents are similar to those of the low-mode Rossby waves, different parts of the current system dominate the advective and PV-gradient modification effects on a single mode. Since the equatorial symmetry of classical equatorial waves alternates between symmetric and antisymmetric with increasing meridional mode number, the currents produce opposite effects on adjacent modes. Meridional mode 1 is slowed primarily by a combination of eastward advection by the Equatorial Undercurrent (EUC) and the PV-gradient decrease at the peaks of the South Equatorial Current (SEC). The mode-2 phase speed, in contrast, is increased primarily by a combination of westward advection by the SEC and the PV-gradient increase at the core of the EUC.

Perturbation solutions are carried to second order in ϵ, the Rossby number of the mean current, and it is shown that this is necessary to capture the full effect of quasi-realistic current systems, which are asymmetric about the equator. Equatorially symmetric components of the current system affect the phase speed at $O(\epsilon)$, but antisymmetric components of the currents and distortions of the wave structures by the currents do not influence the phase speed until $O(\epsilon^2)$.

1. Introduction

The classical theory of equatorial waves in a rest-state ocean is well developed (Matsuno 1966; Moore and Philander 1977), but the strong zonal currents typical of the equatorial oceans are known to affect both the meridional structures and the dispersion relations of these waves. A number of studies have sought to characterize and explain these effects and they are summarized nicely by McPhaden and Ripa (1990). Three theoretical works in particular have illuminated the influence of mean equatorial currents on stable long Rossby waves, our primary concern in this paper. Philander (1979) analyzed the effect of an equatorially symmetric eastward jet [mimicking the Equatorial Undercurrent (EUC)] on the lowest meridional mode in a 1½-layer model. While noting the limitations of this model due to the mismatch between the vertical scales of baroclinic modes and that of the Equatorial Undercurrent, he demonstrated that valuable information about the real ocean could nevertheless be deduced from this approach. Philander showed that the westward phase speed of the meridional-mode-1 Rossby wave was slowed and the peaks in the pressure eigenfunction were shifted poleward by the presence of his idealized undercurrent.

Ripa and Marinone (1983) solved a perturbation problem for 1½-layer linearized waves in the presence of an equatorially symmetric zonal jet with either eastward or westward velocity. They showed the modified eigenfunctions for the meridional-mode-2 long Rossby wave and the modified dispersion relations for the lowest four meridional-mode Rossby waves. The westward phase speeds of meridional modes 1, 3, and 4 were shown

Corresponding author address: Theodore S. Durland, College of Oceanic and Atmospheric Sciences, Oregon State University, Corvallis, OR 97331.
E-mail: tdurland@coas.oregonstate.edu

DOI: 10.1175/2011JPO4503.1

to be faster in the presence of the westward jet than in the presence of the eastward jet, in accordance with the expected Doppler effect. It was less clear whether either jet had any effect on the mode-2 phase speed in the long Rossby wave range. Besides the Doppler shift, Ripa and Marinone demonstrated the effect of the background layer thickness deviations on the speed of inertia–gravity waves. They did not, however, address any additional phase-speed-altering mechanisms in the case of long Rossby waves. An important point that their analysis brought out was that the Doppler shift and the effect of varying background layer thickness depend not just on the magnitude of the background fields but on how these project onto the appropriate eigenfunctions—a point that will play a prominent role in our analysis. The peaks of the mode-2 Rossby wave eigenfunctions in the solutions of Ripa and Marinone (1983) were shifted equatorward in the presence of the westward jet and poleward in the presence of the eastward jet, in agreement with the mode-1 distortion found by Philander (1979).

Proehl (1990) included both the meridional and vertical structure of equatorial currents in his study of their influence on meridional-mode-1 long Rossby waves via WKB solutions, a perturbation expansion, and direct numerical integrations. Using an equatorially symmetric, but otherwise realistic, profile of the Equatorial Undercurrent and overlying South Equatorial Current (SEC), he solved the linearized equations to determine the effects on the lowest few vertical modes. Although distortions of the higher vertical modes were significant, the near-surface changes to the first baroclinic mode were quite similar to those produced by the 1½-layer calculations of Philander (1979). The main effect on the pressure eigenfunction was the poleward migration of the peaks above the undercurrent and a decrease in the wave amplitude below the undercurrent.

In his perturbation solution, Proehl (1990) noted that the Doppler shift is determined by the projection of the mean current onto the squared eigenfunction of zonal velocity or pressure. He also described an additional phase-speed-altering mechanism as ''the projection of the advection of background momentum and density fields by the meridional circulation of the $O(\epsilon)$ wave field (v_0, w_0), upon the wave structures.'' We will show that this is a reasonable qualitative description of the solution's mathematical form but it does not provide useful physical insight into the phase-speed modification.

Surprisingly, none of the aforementioned papers (including the review by McPhaden and Ripa 1990) addressed the impact of the mean current on the ambient potential vorticity (PV) gradient, although this effect is known to be important in the phase-speed modification of midlatitude Rossby waves (e.g., Pedlosky 1987, section 3.18). Chang and Philander (1989) used a semigeostrophic, 1½-layer model to analyze midlatitude Rossby wave rays propagating toward the equatorial zone. They noted that their formulation was not valid in the immediate vicinity of the equator (within 2°–3° of latitude), but their analysis showed the local importance at low latitudes of an ''effective beta'' and an ''effective radius of deformation,'' each of which is modified from the rest-state equivalent by shear in the background current and changes in the background layer thickness. Zheng et al. (1994) included the mean-current curvature (i.e., the relative vorticity gradient of the mean current) in a quasigeostrophic model, in an attempt to predict the phase speeds of near-equatorial Rossby waves. Although neither of the above formulations can be used directly to infer the changes in normal modes that span the equator, they provide an impetus for revisiting the analyses of Ripa and Marinone (1983) and Proehl (1990) with an eye toward extracting more physical insight into phase-speed-modifying mechanisms of the equatorial current system.

Chelton et al. (2003, hereafter C03) numerically solved the 1½-layer equations linearized about zonally and temporally uniform equatorial currents with quasi-realistic meridional profiles to determine the mean-flow-modified eigenfunctions and dispersion relation for the first-meridional-mode, annual long Rossby wave: equivalent to the approach of Philander (1979) but with more realistic current profiles. This was done at numerous longitudinal locations across the Pacific using upper-layer currents obtained by averaging the mean-zonal-current ADCP transects of Johnson et al. (2002) over the upper 250 m. The vertically averaged current systems contain recognizable representations of the eastward-flowing EUC and North Equatorial Countercurrent (NECC) and of the southern (SECS) and northern (SECN) branches of the westward-flowing SEC.

While acknowledging the shortcomings of the 1½-layer approach and the assumption of zonal uniformity, C03 showed that the theoretical pressure eigenfunctions thus derived bear a strong resemblance to the corresponding first empirical orthogonal functions (EOFs) of the altimetrically observed quasi-annual sea surface height (SSH) anomalies between 155° and 110°W in the east-central equatorial Pacific. In their solutions, the mean-current modifications at 140°W include a slowing of the phase speed by ~15% and a distortion of the classical, twin-peaked pressure eigenfunction (symmetric about the equator) such that the amplitude of the distorted wave's northern extremum is roughly twice that of the southern extremum. The mean currents, EOFs and theoretical wave modifications at 140°W were found to be typical of the equatorial Pacific between 155° and 110°W. Farther west, where the current system weakens, the match

between theoretical eigenfunctions and EOFs was not as good. C03 thus highlight both the advantages and the limitations of comparing eigenmode calculations based on the uniform-current assumption with observations in a current system that can change on scales smaller than a wavelength.

The goal of this paper is to illuminate the physical mechanisms by which the equatorial current system alters the phase speeds of long Rossby waves. We will focus on the effects of quasi-realistic, equatorial Pacific currents on the lowest two meridional modes in a 1½-layer format. Higher modes are stable in the 1½-layer model, but their slower phase speeds are probably exceeded by parts of the SEC in its full vertical profile: critical surfaces and wave absorption are likely in the real ocean. The modified phase speeds of modes 1 and 2, however, appear fast enough that these modes can exist as stable waves. Two meridional profiles of zonal currents will be utilized, based on C03's upper-layer currents at 140° and 170°W. The former represent the most robust mean currents found in the equatorial oceans, and the latter represent a transition zone between the central Pacific currents and the weaker currents of the western Pacific. As noted by C03, the effect of the latter currents on the long Rossby waves is qualitatively different than the effect of the former.

The first interesting result of our investigation is that the second meridional mode can be modified in a way that appears to be exactly opposite to the modifications of mode 1. In contrast to the effects on mode 1, described above (and in C03), we show here that the 140°W currents increase the phase speed of mode 2 and distort its SSH structure (antisymmetric in the classical solution) so that the southern extremum is roughly twice as large as the northern one. At 170°W, the mean currents do not produce a significant asymmetry in the eigenfunctions of mode 2 (as with the C03 results for mode 1), but the effect on the dispersion relations of the two modes is still quite different. Although mode 1 is slowed significantly at 170°W, the phase speed of mode 2 changes very little.

Clearly, the effect of the currents on the Rossby waves cannot be encapsulated in a single, catch-all description, and the bulk of this paper is dedicated to developing a formalism by which we can analyze the effects of the current-system components on long Rossby waves. We then use the analysis to explain the reasons for the above-noted differences in the effects of different current systems on a single mode and of a single current system on different modes.

Our approach is a perturbation-expansion formulation similar to those of McPhaden and Knox (1979), Ripa and Marinone (1983), and Proehl (1990) but most closely following the formalism of the second of these studies. The wave currents are small compared to the mean currents, and the Rossby number of the mean currents is also small. The solutions are thus perturbations on the classical Hermite function solutions for an equatorial β-plane basin with no mean flow. The differences between our approach and that of Ripa and Marinone (1983) are several. First, they examined the effect of a single Gaussian jet, whereas we use the quasi-realistic current systems of C03. Second, we extend our linearized analysis to second order in the perturbation parameter, which provides important insights that are not available with only the lower order solution. Finally, we recast the mathematical expressions for the perturbation corrections to reflect the expected physical mechanisms by which the mean currents affect Rossby wave speeds: advection, modification of the background PV gradient, and modification of the local deformation radius. The various expressions are then evaluated numerically and analyzed graphically for an enhanced understanding of the dynamics that contribute to the wave speed modifications.

Most of our solutions are calculated at the annual period but are representative of the entire long Rossby wave domain for both meridional modes, that is, all wave periods intraseasonal (~60 days) or longer. The only noticeable change throughout this range is the ratio between the meridional-wave-velocity amplitude and that of the zonal wave velocity, a ratio that decreases with increasing period.

We do not consider zonal and temporal variability in the background currents, and the 1½-layer approach of course ignores the effects of vertical shear on the waves. Care must therefore be taken in applying our results to the real equatorial ocean where zonal currents have strong vertical shears, annual and interannual variability, and zonal scales shorter than the wavelengths of long Rossby waves at all but perhaps the intraseasonal period (Johnson et al. 2002).

There is, nevertheless, ample justification for our approach. Our knowledge of oceanic dynamics has often been built on idealized analytical models that do not fully represent the real ocean but can identify basic physical mechanisms in ways that observations or complex numerical models cannot. Fortunately, the insights gained often have proven useful well outside the strict validity range of the models. As previously noted, for instance, the 1½-layer model can capture the essence of changes to the near-surface pressure field of the first-baroclinic-mode, first-meridional-mode long Rossby wave found in the calculations of Proehl (1990) involving quasi-realistic vertical as well as meridional shear. We are motivated by the fact that the effect of strong meridional shear on oceanic, equatorial Rossby modes has yet to be

described in terms of modifications to the ambient PV field. In this paper, we begin to fill this gap with physical understanding at the most basic level.

Section 2 presents the nondimensional equations with which we will work and the background current profiles at 140° and 170°W, which will be used in our analysis. In addition, numerical eigenvalue solutions for modes 1 and 2 in the two different current systems will be shown to set up the specific questions that we wish to answer with the perturbation analysis. The perturbation problem is developed in section 3, and we present the solutions in section 4. Section 5 contains an analysis of how the various aspects of the mean current system contribute to dispersion-relation modifications, and section 6 summarizes our results.

2. Equations and numerical solutions

a. Equations

Our mathematical framework is the nondimensional shallow-water equations on the equatorial β plane,

$$\partial_t \tilde{\mathbf{u}} + \tilde{\mathbf{u}} \cdot \nabla \tilde{\mathbf{u}} + y\mathbf{k} \times \tilde{\mathbf{u}} + \nabla \tilde{\eta} = 0 \tag{1}$$

and

$$\partial_t \tilde{\eta} + \nabla \cdot [(1 + \tilde{\eta})\tilde{\mathbf{u}}] = 0, \tag{2}$$

which represent the dynamics of a 1½-layer model with mean layer thickness H_0 and reduced gravity γ. The layer thickness deviation $\tilde{\eta}$ was normalized by H_0 while the vector velocity $\tilde{\mathbf{u}}$ (with zonal and meridional components $\tilde{u}$ and $\tilde{v}$) was normalized by the Kelvin wave speed, $c = \sqrt{\gamma H_0}$. Zonal and meridional distances x and y were normalized by the equatorial deformation radius $L_e = \sqrt{c/\beta}$, and time t was normalized by the equatorial time scale $T_e = 1/\sqrt{\beta c}$, where β is the meridional derivative of the Coriolis parameter at the equator. We will assume an equatorial deformation radius of 340 km (3.1° latitude), which corresponds to a Kelvin wave speed of 2.7 m s^{-1}, typical of the first baroclinic mode in the central equatorial Pacific (Chelton et al. 1998). The corresponding time scale is 1.5 days.

Consider a small-amplitude wave field superimposed on a zonal current system that is independent of x and t,

$$\begin{pmatrix} \tilde{u} \\ \tilde{v} \\ \tilde{\eta} \end{pmatrix} = \epsilon \left[\begin{pmatrix} \widehat{U}(y) \\ 0 \\ \widehat{\delta H}(y) \end{pmatrix} + \mu \begin{pmatrix} \hat{u}(x,y,t) \\ \hat{v}(x,y,t) \\ \hat{\eta}(x,y,t) \end{pmatrix} \right], \tag{3}$$

where the variable terms on the right-hand side (rhs) are $O(1)$. The parameter $\epsilon = \max(|U_*|)/c$ is the equatorial Rossby number of the mean current (the asterisk subscript indicates a dimensional variable). The scale separation between the wave field and the mean-current field is μ, and we assume that $\mu \ll \epsilon < 1$.

The mean current is geostrophic:

$$y\widehat{U} + \widehat{\delta H}' = 0, \tag{4}$$

where the prime indicates a derivative with respect to y. With this constraint, the equations are

$$\left[\begin{pmatrix} \partial_t & -y & \partial_x \\ y & \partial_t & \partial_y \\ \partial_x & \partial_y & \partial_t \end{pmatrix} + \epsilon \begin{pmatrix} \widehat{U}\partial_x & \widehat{U}' & 0 \\ 0 & \widehat{U}\partial_x & 0 \\ \widehat{\delta H}\partial_x & (\widehat{\delta H}' + \widehat{\delta H}\partial_y) & \widehat{U}\partial_x \end{pmatrix} + O(\epsilon\mu) \right] \begin{pmatrix} \hat{u} \\ \hat{v} \\ \hat{\eta} \end{pmatrix} = 0, \tag{5}$$

where the $O(\epsilon\mu)$ terms are the nonlinear wave–wave interactions. Neglecting these small terms gives us a linear system that we Fourier transform in x and t using the convention

$$(\hat{u}\,\hat{v}\,\hat{\eta}) = \int\int [u(y)\, v(y)\, \eta(y)] e^{i(kx - \sigma t)}\, dk\, d\sigma. \tag{6}$$

The zonal wavenumber k and frequency σ have been nondimensionalized by L_e^{-1} and T_e^{-1}, respectively.

For a specific value of k, (5) becomes the linear eigenvalue problem:

$$(\mathcal{L}_k - i\sigma + \epsilon\mathcal{N}_k)[u(y)v(y)\eta(y)]^{\mathrm{T}} = 0, \tag{7}$$

with boundedness conditions on $-\infty < y < \infty$. The operator $(\mathcal{L}_k - i\sigma)$ is the linear shallow-water operator, and $\mathcal{N}_k$ represents the linearized effects of the mean current,

$$(\mathcal{L}_k - i\sigma) = \begin{pmatrix} -i\sigma & -y & ik \\ y & -i\sigma & \dfrac{d}{dy} \\ ik & \dfrac{d}{dy} & -i\sigma \end{pmatrix},$$

$$\mathcal{N}_k = \begin{pmatrix} ik\widehat{U} & \widehat{U}' & 0 \\ 0 & ik\widehat{U} & 0 \\ ik\widehat{\delta H} & \left(\widehat{\delta H}' + \widehat{\delta H}\dfrac{d}{dy}\right) & ik\widehat{U} \end{pmatrix}. \tag{8}$$

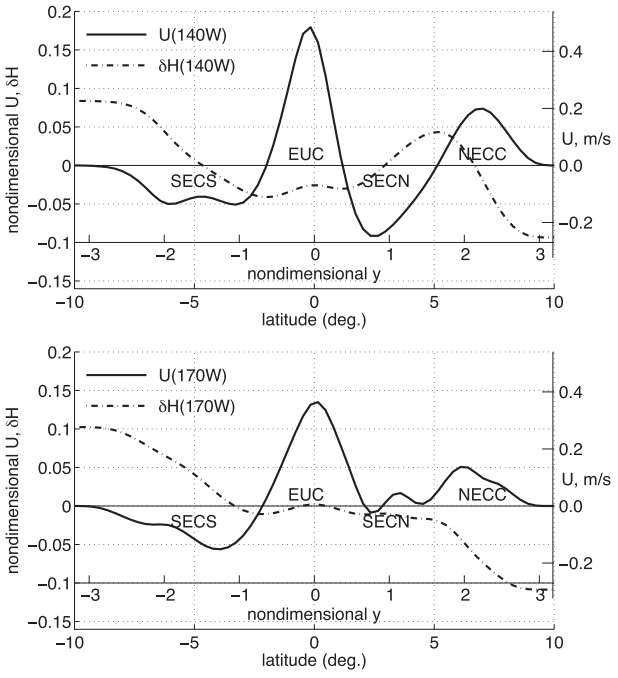

FIG. 1. Equatorial zonal-current systems at (top) 140° and (bottom) 170°W from C03 (based on average ADCP transects of Johnson et al. 2002).

Defining $U = \epsilon\widehat{U}$ and $\delta H = \epsilon\widehat{\delta H}$, (7) is written in the familiar form for the shallow-water equations linearized about a mean zonal current,

$$-i\sigma u + ikUu - (y - U')v + ik\eta = 0, \tag{9}$$

$$-i\sigma v + ikUv + yu + \eta' = 0, \tag{10}$$

and

$$-i\sigma\eta + ikU\eta + (1 + \delta H)iku + [(1 + \delta H)v]' = 0. \tag{11}$$

Equations (9)–(11) are discretized on a staggered grid with a dimensional grid spacing of $L_e/10$; all dependent variables are constrained to vanish at ±20° latitude. The matrix eigenvalue problem is then solved numerically with k fixed and σ being the eigenvalue.

b. Background currents

The mean upper-layer current structures that we will use, along with the corresponding mean layer thickness deviations, are displayed in Fig. 1. They are smoothed and tapered versions of the currents used by C03 for 140° (top panel) and 170°W (bottom panel). The structure at 140°W is typical of the equatorial Pacific mean currents from 155° to 110°W, and it is in this span where distortions of the rest-state eigensolutions by the mean-flow effects are maximal (C03). We include consideration of the 170°W currents because the distortions of the eigensolutions are quite different at this longitude in spite of the SECS, EUC, and NECC magnitudes being of the same order as at 140°W. As noted by C03, the biggest difference between the two profiles is the absence of a SECN at 170°W. Other differences that appear to have less of an effect on the waves are the slight displacement of the EUC core south of the equator at 140°W (in contrast to the more equatorially symmetric EUC at 170°W) and the more equatorward location of the NECC peak at 170°W relative to 140°W.

The deviation $\delta H(y)$ can only be determined from (4) to within an arbitrary constant, dependent on the latitude where we assume the background layer thickness to be equal to the rest-state thickness H_0. We have chosen for H_0 the average layer thickness over the span of the low-mode waves: $|y| < 3$ ($\approx \pm 9°$ latitude). This is roughly equivalent to determining the equatorial deformation radius and time scale from the average hydrography over the equatorial waveguide. An inspection of Fig. 1 shows that choosing H_0 at any specific latitude within about 2° of the equator would change its value by less than 6%, corresponding to a difference of less than 3% in the value of c and less than 2% in the value of L_e. These differences would be insignificant on the scale of the comparisons that we will make between rest-state and mean-current-modified waves.

c. Dispersion relations

The dispersion curves for both the classical rest-state solutions and those modified by the two current systems can be seen in Fig. 2. As noted in the introduction, mode-1 long waves are slowed by both current systems, whereas mode-2 long-wave speeds are increased at 140°W and barely affected at 170°W. In addition to highlighting the specific physical mechanisms involved, our perturbation analysis will address the obvious questions posed by this figure: why does a single current system affect the two adjacent modes so differently and why do the two mostly similar current systems affect a single mode so differently?

d. Eigenfunctions

Although our primary focus in this paper is not the eigenfunction distortions, we will see that they play a role in the dispersion-relation modifications, and it is worthwhile to understand the qualitative nature of the distortions. The numerical eigenfunction solutions also provide a benchmark against which we can judge the adequacy of the perturbation solutions.

The rest-state and 140°W distorted eigenfunctions at the annual period appear in Fig. 3. Note that v is an order

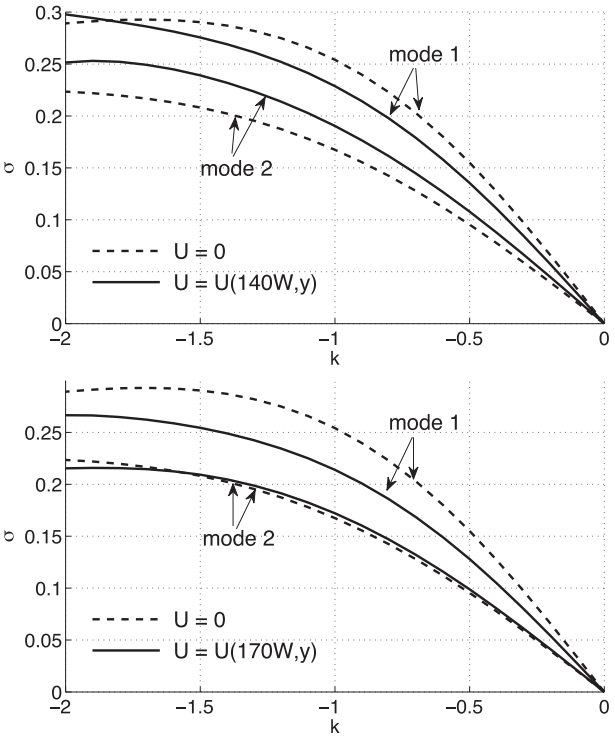

FIG. 2. Rossby wave dispersion curves for the lowest two meridional modes at (top) 140° and (bottom) 170°W. Solid curves represent numerical solutions of shallow-water equations linearized about the mean currents. Dashed curves are the classical Hermite solutions for no mean flow. In each panel the top two curves are mode-1 solutions, whereas the bottom two curves are mode-2 solutions. Note the opposite effects of the current systems on the phase speeds of the two adjacent meridional modes.

of magnitude smaller than u and η. Although the ratio of $|u|_{\max}$ to $|v|_{\max}$ increases with increasing wave period, the relative structures seen in Fig. 3 remain virtually unchanged for all periods intraseasonal and longer. The previously discussed asymmetry in the η structure of mode 1 at 140°W is clearly seen (cf. Fig. 20 of C03), with the northern peak having roughly twice the amplitude of the southern peak. The asymmetry introduced in the η eigenfunction of mode 2 is complementary to that of mode 1: the southern peak has roughly twice the amplitude of the northern peak. The peaks in the η structure of mode 1 at 140°W are shifted poleward from the classical solutions by 1°–2° of latitude, as noted by C03. This is also true of the northern peak of mode 2, but the southern peak is shifted slightly equatorward.

Figure 4 shows the rest-state and mean-current-modified eigenfunctions at 170°W in the same format as Fig. 3. The striking asymmetries seen at 140°W are not present at 170°W, with the most noticeable changes in the η eigenfunctions being the poleward shifts of the peaks and the widening of the northern peak of mode 1.

3. Perturbation expansion

We seek to understand the current-modified solutions as perturbations on the familiar rest-state solutions, so we consider a weak mean current system, $\epsilon \ll 1$. Inspection of Fig. 1 suggests that, in our full-strength current scenarios, we will be dealing with a value of ϵ that is $O(10^{-1})$.

In (7) both σ and the wave vector are expanded in powers of the Rossby number,

$$\sigma = \sum_{p=0}^{\infty} \sigma_p \epsilon^p, \quad (u\, v\, \eta) = \sum_{p=0}^{\infty} (u_p\, v_p\, \eta_p)\epsilon^p. \tag{12}$$

At $O(1)$ we have the rest-state equation:

$$(\mathcal{L}_k - i\sigma_0)(u_0\, v_0\, \eta_0)^{\mathrm{T}} = 0; \tag{13}$$

at the higher orders:

$$\mathcal{L}_k \begin{pmatrix} u_p \\ v_p \\ \eta_p \end{pmatrix} + \mathcal{N}_k \begin{pmatrix} u_{p-1} \\ v_{p-1} \\ \eta_{p-1} \end{pmatrix} - i \sum_{q=0}^{p} \sigma_q \begin{pmatrix} u_{p-q} \\ v_{p-q} \\ \eta_{p-q} \end{pmatrix} = 0, \quad p > 0. \tag{14}$$

The subscripts on the operators $\mathcal{L}_k$ and $\mathcal{N}_k$ remind us that the formulation is for a specific value of the zonal wavenumber k.

We will expand $(u_p\, v_p\, \eta_p)$ in the eigenvectors of the $O(1)$ rest-state problem, (13). While the separate orders of the perturbation-expansion solutions are identified with single subscripts, the eigenvalues and eigenfunctions of (13) will be labeled with double subscripts,

$$\sigma_{mn}, \quad (u_{mn}\, v_{mn}\, \eta_{mn}), \quad m = -1, 0, 1, 2, \cdots; \quad n = 1, 2, 3, \tag{15}$$

to identify the three wave types and the infinite number of meridional modes that are solutions to (13). These are the classical equatorial β-plane solutions on the rest state, which are based on Hermite functions (Moore and Philander 1977). The first subscript, m, indicates the meridional mode number. For $m \geq 1$, a single zonal wavenumber is associated with three solutions to the frequency equation, representing the inertia–gravity wave with eastward phase propagation ($n = 1$), the Rossby wave ($n = 2$) and the inertia–gravity wave with westward phase propagation ($n = 3$). For $m = 0$, the unbounded plane admits only the Yanai (or mixed Rossby–gravity) wave solution with eastward ($n = 1$) or westward ($n = 3$) phase propagation. The eastward propagating Kelvin wave is identified by $m = -1, n = 1$ and is the only wave type associated with this value of m. The $m = -1, n = 2, 3$ vectors and the $m = 0, n = 2$ vector are identically zero. The combination of all the above meridional modes and wave types forms

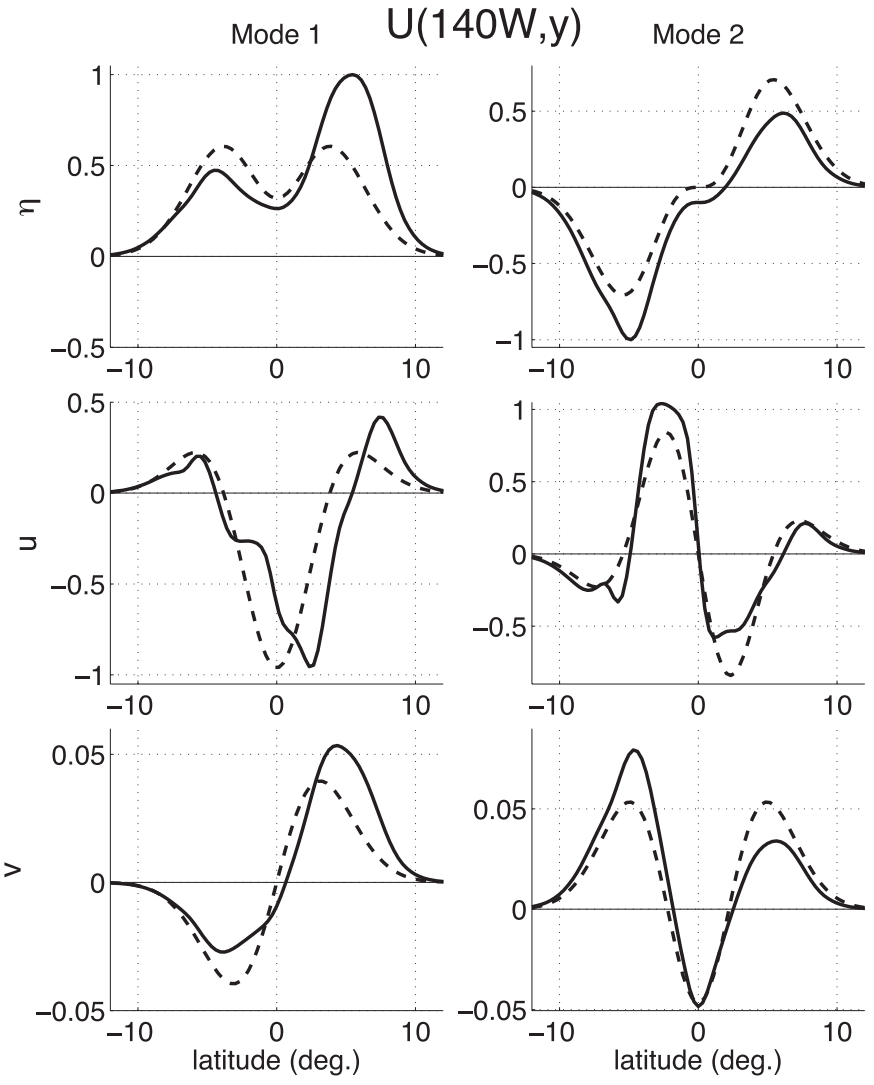

FIG. 3. Long Rossby wave (top) η, (middle) u, and (bottom) v eigenfunctions at the annual period: meridional (left) mode 1 and (right) mode 2. Solid curves represent numerical solutions of shallow-water equations linearized about the currents at 140°W. Dashed curves are classical solutions for no mean flow.

a complete orthogonal basis (Ripa 1982) in which we can expand the higher-order perturbation wave vectors. The nonzero eigenvectors are normalized so that

$$\int_{-\infty}^{\infty} dy |u_{mn}|^2 + |v_{mn}|^2 + |\eta_{mn}|^2 = 1. \qquad (16)$$

We emphasize some important properties of the Hermite solution wave vectors. First, the zonal velocity and pressure, u_{mn} and η_{mn}, are 90° out of phase with the meridional velocity v_{mn}. We follow the usual convention and consider v_{mn} to be real, while u_{mn} and η_{mn} are imaginary. Second, for $m \geq 0$, v_{mn} is either symmetric or antisymmetric about the equator, and both u_{mn} and η_{mn} have the opposite symmetry to v_{mn} (note that $v_{-1,1} \equiv 0$). Thus, the wave vector $(u_{mn}\, v_{mn}\, \eta_{mn})$ can be assigned a single symmetry, with the relative symmetries of the individual components implied. We will use the symmetry of η_{mn} to label the symmetry of the wave vector. Third, the symmetry of these classical wave vectors alternates with increasing meridional-mode number: η_{mn} is symmetric about the equator when m is odd and antisymmetric about the equator when m is even.

The $O(1)$ solution is equated to a single Hermite mode of unit amplitude:

$$\sigma_0 = \sigma_{MN}, \quad (u_0\, v_0\, \eta_0) = (u_{MN}\, v_{MN}\, \eta_{MN}), \qquad (17)$$

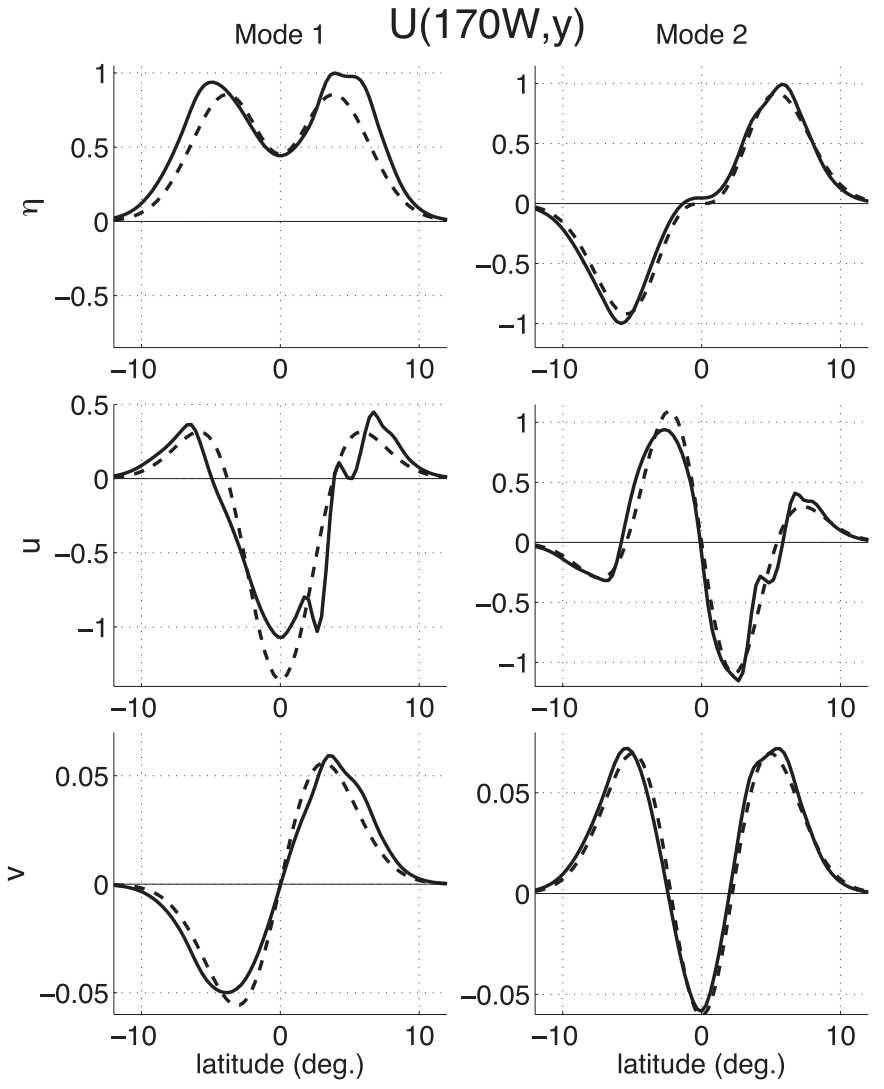

FIG. 4. As in Fig. 3 but for mean currents at 170°W.

where M and N are specific values of m and n identifying the particular wave under consideration. The $O(\epsilon^p)$ wave vector corrections are then expanded in the Hermite eigenvectors of (13),

$$(u_p\, v_p\, \eta_p) = \sum_{m,n} A_{mn}^{(p)} (u_{mn}\, v_{mn}\, \eta_{mn}). \tag{18}$$

By changing the orders of the perturbation (12) and eigenvector (18) summations, we can show that

$$A_{MN}^{(p)} = 0, \quad p \neq 0; \tag{19}$$

that is, the Hermite mode MN enters the solution only at $O(1)$. For a consistent formalism, (18) can also be applied at $O(1)$, with

$$A_{mn}^{(0)} = \begin{cases} 1, & m = M \quad \text{and} \quad n = N \\ 0, & \text{otherwise.} \end{cases} \tag{20}$$

Employing the expansion (18) in (14), multiplying on the left by the complex conjugate of a Hermite wave vector $(u_{st}\, v_{st}\, \eta_{st})^*$, and integrating over the domain, we have for $p > 0$

$$\sigma_p = -i \sum_{m,n} A_{mn}^{(p-1)} \int_{-\infty}^{\infty} (u_{MN} v_{MN} \eta_{MN})^* \mathcal{N}_k \begin{pmatrix} u_{mn} \\ v_{mn} \\ \eta_{mn} \end{pmatrix} dy, \quad st = MN \tag{21}$$

and

$$A_{st}^{(p)} = \frac{1}{\sigma_{st} - \sigma_{MN}}\left[\sum_{q=1}^{p}\sigma_q A_{st}^{(p-q)} + i\sum_{m,n}A_{mn}^{(p-1)}\int_{-\infty}^{\infty}(u_{st}v_{st}\eta_{st})^*\mathcal{N}_k\begin{pmatrix}u_{mn}\\ v_{mn}\\ \eta_{mn}\end{pmatrix}dy\right], \quad st \neq MN. \tag{22}$$

We carry the expansion to $O(\epsilon^4)$ at 140°W to check on the convergence of the perturbation series, but we attempt to draw physical meaning only from $O(\epsilon)$ and $O(\epsilon^2)$, for which the expressions are

$$\sigma_1 = -i\int_{-\infty}^{\infty}(u_{MN}v_{MN}\eta_{MN})^*\mathcal{N}_k\begin{pmatrix}u_{MN}\\ v_{MN}\\ \eta_{MN}\end{pmatrix}dy, \tag{23}$$

$$A_{st}^{(1)} = \frac{i}{\sigma_{st} - \sigma_{MN}}\int_{-\infty}^{\infty}(u_{st}v_{st}\eta_{st})^*\mathcal{N}_k\begin{pmatrix}u_{MN}\\ v_{MN}\\ \eta_{MN}\end{pmatrix}dy, \quad st \neq MN, \tag{24}$$

$$\sigma_2 = -i\sum_{m,n}A_{mn}^{(1)}\int_{-\infty}^{\infty}(u_{MN}v_{MN}\eta_{MN})^*\mathcal{N}_k\begin{pmatrix}u_{mn}\\ v_{mn}\\ \eta_{mn}\end{pmatrix}dy, \tag{25}$$

and

$$A_{st}^{(2)} = \frac{1}{\sigma_{st} - \sigma_{MN}}\left[\sigma_1 A_{st}^{(1)} + i\sum_{m,n}A_{mn}^{(1)} \times \int_{-\infty}^{\infty}(u_{st}\,v_{st}\,\eta_{st})^*\mathcal{N}_k\begin{pmatrix}u_{mn}\\ v_{mn}\\ \eta_{mn}\end{pmatrix}dy\right], \quad st \neq MN. \tag{26}$$

The above expressions are general for all equatorial waves. In principle, all wave types can contribute to the modification of a particular eigenmode; indeed, all are required for completeness of the basis. Nevertheless, the inverse frequency difference that leads the expressions for the expansion coefficients appears to limit the contributions to modes of a similar wave type (a point also made by Proehl 1990). In our long-Rossby-wave calculations, we find that the contributions to (18) of the inertia–gravity modes ($n = 1, 3$) are negligible.

Symmetry considerations

If $\widehat{U}$ (and consequently $\widehat{\delta H}$) is symmetric about the equator, then multiplying a Hermite basis vector of a particular y symmetry by $\mathcal{N}_k$ will produce a new vector with the same symmetry. This is most easily seen by considering the symmetric part of the background field, $\widehat{U}_S = [\widehat{U}(y) + \widehat{U}(-y)]/2$ and $\widehat{\delta H}_S = [\widehat{\delta H}(y) + \widehat{\delta H}(-y)]/2$, with the corresponding operator $\mathcal{N}_{kS} = \mathcal{N}_k(\widehat{U}_S, \widehat{\delta H}_S)$ and defining the product

$$\begin{pmatrix}a\\ b\\ c\end{pmatrix} = \mathcal{N}_{kS}\begin{pmatrix}u_+\\ v_-\\ \eta_+\end{pmatrix} = ik\widehat{U}_S\begin{pmatrix}u_+\\ v_-\\ \eta_+\end{pmatrix} + \begin{pmatrix}(\widehat{U}_S)'v_-\\ 0\\ ik\widehat{\delta H}_S u_+ + (\widehat{\delta H}_S v_-)'\end{pmatrix}. \tag{27}$$

In (27), $(u_+, v_-, \eta_+)^{\mathrm{T}}$ represents a basis vector of a particular symmetry, where the subscript + can represent either a y-symmetric or a y-antisymmetric field, while the subscript − represents the opposite symmetry. Multiplication of the basis vector by $\widehat{U}_S$ (first term on the rhs) clearly leaves the symmetry of the vector unchanged. In the second term on the rhs, $(\widehat{U}_S)'$ is antisymmetric, so $(\widehat{U}_S)'v_-$ has the same symmetry as u_+. Likewise, both $\widehat{\delta H}_S u_+$ and $(\widehat{\delta H}_S v_-)'$ have the same symmetry as η_+, so the product vector $(a\ b\ c)^{\mathrm{T}}$ has the same symmetry as the basis vector $(u_+\ v_-\ \eta_+)^{\mathrm{T}}$.

A similar analysis shows that, if $\widehat{U}$ is antisymmetric in y ($\widehat{U} = \widehat{U}_A$ and $\mathcal{N}_k = \mathcal{N}_{kA}$), then multiplication of an eigenvector by $\mathcal{N}_k$ changes the symmetry. Consequently, the operator $\mathcal{N}_k$ can be thought of as having the same y symmetry as $\widehat{U}$ (note that we refer to the operational effect of $\mathcal{N}_k$ on the basis vectors and not to the matrix symmetry of $\mathcal{N}_k$).

If $\mathcal{N}_k(\widehat{U})$ is symmetric and $(u_{st}\,v_{st}\,\eta_{st})$ has the opposite symmetry to our $O(1)$ solution, $(u_{MN}\,v_{MN}\,\eta_{MN})$, then the integrand in (24) will be antisymmetric and $A_{st}^{(1)}$ will vanish. At $O(\epsilon)$, therefore, the symmetric part of $\widehat{U}$ produces only eigenfunction corrections that have the same symmetry as the $O(1)$ solution, a point that was made by Ripa and Marinone (1983). Conversely, the antisymmetric part of $\widehat{U}$ will result in $O(\epsilon)$ contributions that have the opposite symmetry to the $O(1)$ solution. Asymmetries in the eigenfunctions can thus be produced at $O(\epsilon)$ only by the antisymmetric part of $\widehat{U}$. By the same logic, we see in (23) that only the symmetric part of $\widehat{U}$ can contribute to changes in the dispersion relation at $O(\epsilon)$.

At $O(\epsilon^2)$, both symmetric and antisymmetric parts of $\widehat{U}$ can contribute to the frequency correction. Suppose that $\mathcal{N}_k$ has an antisymmetric part that generates an $O(\epsilon)$

eigenfunction correction $A^{(1)}_{mn}(u_{mn}\, v_{mn}\, \eta_{mn})$ that has the opposite symmetry of the $O(1)$ solution $(u_{MN}\, v_{MN}\, \eta_{MN})$. In (25), the antisymmetric part of $\mathcal{N}_k$ operating on $(u_{mn}\, v_{mn}\, \eta_{mn})$ will produce a vector with the same symmetry as $(u_{MN}\, v_{MN}\, \eta_{MN})$, resulting in a symmetric integrand. There will be a nonzero contribution to the frequency modification at $O(\epsilon^2)$ due to the interaction of the antisymmetric part of the mean current with the asymmetrizing mode *mn*.

We can think of the situation heuristically as an interaction in which a local contribution to the phase-speed change depends on both the local strength of the phase-speed-changing mechanism of the mean current and the local relative magnitude of the wave vector. At $O(1)$, the magnitudes of all Hermite eigenvectors are symmetric about the equator, and phase-speed-altering aspects of the mean flow that are antisymmetric about the equator cancel themselves in the integral, producing no net effect. Once an asymmetry is introduced in the wave vector, however, the effect of the antisymmetric part of $\widehat{U}$ will no longer balance between the two hemispheres, and a net change in phase speed will result. The asymmetry introduced in the wave vector at $O(\epsilon)$ allows both the antisymmetric and the symmetric part of $\widehat{U}$ to affect the phase speed at $O(\epsilon^2)$.

More generally, the $O(\epsilon)$ solution gives us only the effect on phase speed of the interaction between the background currents and the unmodified wave vectors. As the wave vectors themselves are changed, we must consider the interaction between the background currents and the distorted wave vectors, whether or not the distortions involve asymmetries. This effect enters into the perturbation solution only at $O(\epsilon^2)$.

4. Perturbation solutions

In the following discussion, the $O(\epsilon^p)$ correction to frequency, for instance, refers to either σ_p or $\sigma_p\epsilon^p$, with the context making the choice clear. The $O(\epsilon^p)$ frequency solution, on the other hand, refers to $\sigma = \sum_{q=0}^{p}\sigma_q\epsilon^q$. The $O(1)$, $O(\epsilon)$, and $O(\epsilon^2)$ perturbation solutions with $\epsilon\widehat{U} = U(140°\text{W}, y)$ and $\epsilon\widehat{U} = U(170°\text{W}, y)$ are displayed in Figs. 5–7. The numerical solutions from section 2 are also displayed as ''ground truths.'' The eigenfunctions have been normalized so that the maximum amplitude of η is unity for both the numerical and $O(\epsilon^2)$ perturbation solutions. The eigenfunctions of the lower-order perturbation solutions are normalized by the same constant as those of the $O(\epsilon^2)$ solution.

We can see in Fig. 5 that the small change in mode-2 phase speed for long Rossby waves at 170°W is reproduced quite well by the $O(\epsilon)$ solution. In the other scenarios there is a larger change in phase speed and the $O(\epsilon)$ solution overestimates the change. At $O(\epsilon^2)$, the match is quite good between the perturbation and numerical solutions for long Rossby waves in all cases. Inspection of (7) and (8) shows that the size of much of the mean-current effect is ϵk, and Fig. 5 confirms that the accuracy of the $O(\epsilon^2)$ solution degrades as $|k|$ exceeds 1.

Figure 6 shows the 140°W η, u, and v eigenfunctions, with (18) summed up to $m = 20$ for both $O(\epsilon)$ and the $O(\epsilon^2)$ corrections. The $O(\epsilon)$ solution anticipates the sense in which the eigenfunctions are distorted but underestimates the magnitude in each case. The $O(\epsilon^2)$ solution provides a reasonable match with the numerical solutions, although it does not quite capture the extent of the asymmetry in the mode-1 η eigenfunction and some of the smaller-scale distortions of the u eigenfunction. Most of the η and v distortion is captured by summing (18) up to only $m = 5$ (not shown), with higher-mode contributions necessary only for a reasonable match of the u eigenfunction.

The eigenfunction solutions for $U(170°\text{W}, y)$ are displayed in Fig. 7, with 30 Rossby modes contributing to the perturbation solutions. The small asymmetry and poleward shift of the η peaks are produced by a few low-mode contributions, but the broadening of the northern η peaks and the small-scale structure in u require the contributions of modes between 10 and 30. Summing (18) up to $m = 300$ does not visibly improve the eigenfunction approximations at either 140° or 170°W.

At 170°W the $O(\epsilon^2)$ corrections are appropriately an order of magnitude smaller than the $O(\epsilon)$ corrections, but at 140°W the two corrections are the same order of magnitude. This raises questions about the convergence of the perturbation solution, and in Fig. 8 we display solutions up to $O(\epsilon^4)$ for the η eigenfunctions and the dispersion relations of modes 1 and 2 at 140°W. The perturbation-solution eigenfunctions have been normalized so that the maximum amplitude of the $O(\epsilon^4)$ solution matches that of the numerical solution. To better show small discrepancies, the perturbation-solution dispersion curves have been normalized by the numerical solutions. The eigenfunction solutions and the frequencies in the long Rossby wave range appear to be converging well. The 5%–10% underestimate of the mode-1 asymmetry in η at $O(\epsilon^2)$, noted in connection with Fig. 6, is more clearly seen at this scale. Throughout the long Rossby wave range, however, the $O(\epsilon^2)$ frequency solutions are within 1%–2% of the $O(\epsilon^4)$ solutions. The perturbation-solution frequencies appear to be converging to a limit 1%–2% higher than the numerical-solution frequencies, probably owing to resolution in the required numerical integrations. Both the numerical eigenvalue problem and the numerical integrations of (23)–(26) were discretized on

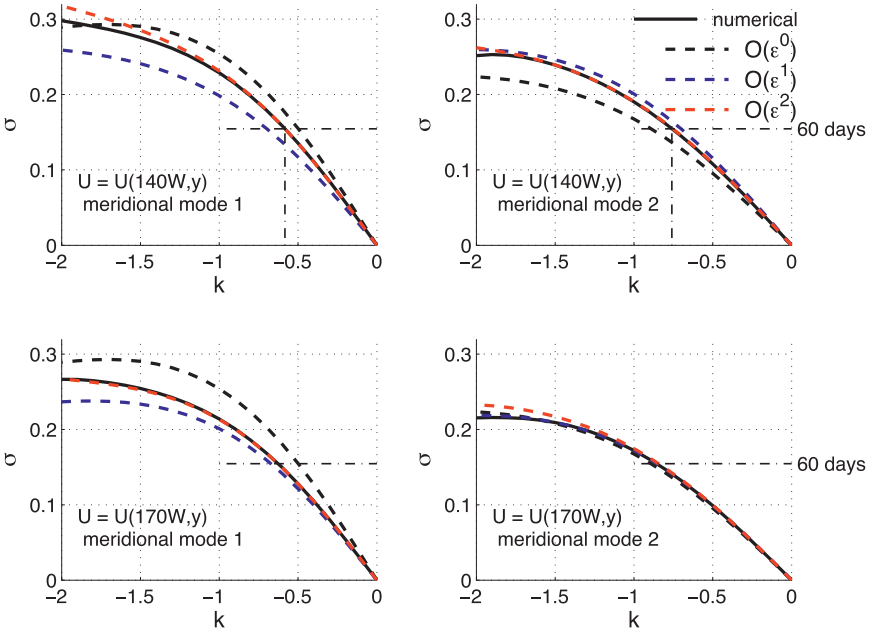

FIG. 5. Rossby wave dispersion curves for meridional (left) mode 1 and (right) mode 2: (top) $U = U(140°\text{W}, y)$ and (bottom) $U = U(170°\text{W}, y)$. Dashed black curves: $O(1)$ (Hermite) solutions; dashed blue curves: $O(\epsilon)$ solutions; and dashed red curves: $O(\epsilon^2)$ solutions. Numerical solutions are represented by black solid curves. The light dashed–dotted horizontal lines mark our nominal short-period limit (60 days) to the long Rossby wave range. The dashed–dotted vertical lines (upper two panels) mark the wavenumbers at which the numerical dispersion curves cross the 60-day limit (for use in Fig. 8).

a grid spacing of $0.1L_e$ ($\approx 0.3°$ latitude). Halving this spacing decreases the discrepancy between the numerical and $O(\epsilon^4)$ frequencies to less than 1%.

The $O(\epsilon^2)$ solutions, particularly for frequency, are sufficiently close to convergence for our purposes. We are less likely to succeed at extracting physical insights from the higher order solutions, and through the remainder of the paper we will discuss solutions no higher than $O(\epsilon^2)$. We speculate that the large magnitude of the $O(\epsilon^2)$ correction and the subsequent rapid convergence is related to the matter discussed in the symmetry considerations subsection of section 3, as well as to the eigenvalue–eigenfunction connection. We have shown that $O(\epsilon^2)$ is the lowest order at which asymmetries in the current can affect the frequency calculation, and it is also the lowest order at which changes in the eigenfunctions affect changes in the frequency and vice versa. As such, the $O(\epsilon^2)$ correction is a fundamental addition to the dynamics at the lowest order in which it can appear.

5. Physical mechanisms for phase speed modification

With some confidence that the perturbation solution reproduces the important modifications of long Rossby waves by mean currents typical of the equatorial Pacific, we turn now to extracting physical insight from the equations for the frequency correction.

a. *Interpretation of the $O(\epsilon)$ correction*

Carrying out the multiplications in (23), we have

$$\frac{\sigma_1}{k} = \int_{-\infty}^{\infty} \widehat{U}(|u_0|^2 + |v_0|^2 + |\eta_0|^2)\, dy - \frac{i}{k}\int_{-\infty}^{\infty} (\widehat{U}' u_0^* v_0 + (\widehat{\delta H} v_0)' \eta_0^*)\, dy + \int_{-\infty}^{\infty} \widehat{\delta H} \eta_0^* u_0\, dy. \tag{28}$$

This relation was derived by Ripa and Marinone (1983) and a similar one by Proehl (1990) in his model with both meridional and vertical structure. The first integral on the rhs is clearly the effect of advection by the mean current. Were the current uniform in y, this term would just be the Doppler shift $\widehat{U}$ [remembering that $\int(|u_0|^2 + |v_0|^2 + |\eta_0|^2)\, dy = 1$]. The form of this term points to an important principle: it is not just the strength of the mean current that matters but how it projects onto the square of the total wave field, $(|u_0|^2 + |v_0|^2 + |\eta_0|^2)$.

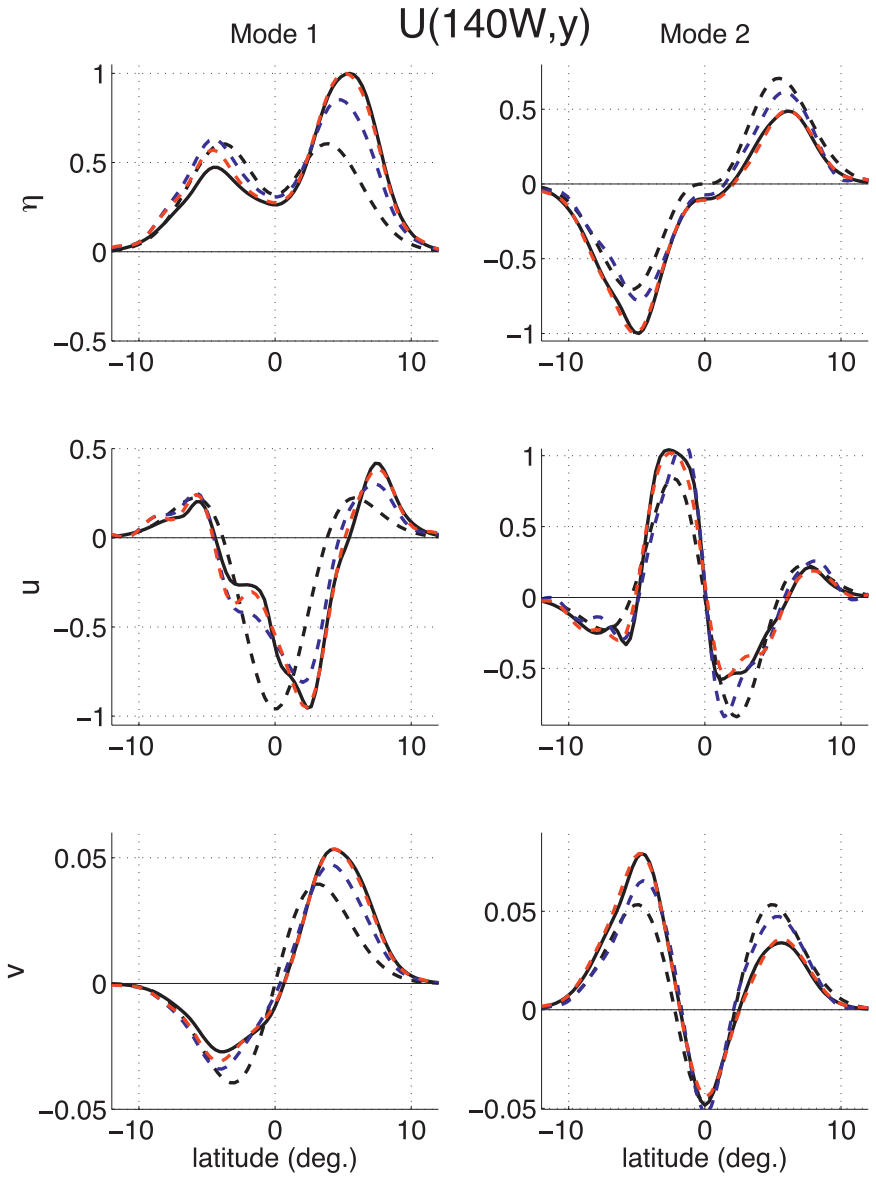

FIG. 6. Long Rossby wave (top) η, (middle) u, and (bottom) v eigenfunctions for $U = U(140°\text{W}, y)$: meridional (left) mode 1 and (right) mode 2 at the annual period. Twenty Hermite Rossby modes are included in the correction expansions. Dashed black curves: $O(1)$ (Hermite) solutions; dashed blue curves: $O(\epsilon)$ solutions; and dashed red curves: $O(\epsilon^2)$ solutions. Numerical solutions are represented by black solid curves.

In the case of short Rossby waves (as demonstrated by Ripa and Marinone 1983), the net advection is determined by the projection of the mean current onto the squared meridional velocity structure since this component dominates the wave vector. For long Rossby waves, however, $|v_0| \ll |u_0|$ and the net advection is determined by the projection of $\hat{U}$ onto $(|u_0|^2 + |\eta_0|^2)$. Proehl (1990) appears to have concluded similarly, but it is easy to misread his results as emphasizing the projection of $\hat{U}$ onto $|v_0|^2$ (a misinterpretation made by McPhaden and Ripa 1990). The difference is significant because the symmetry of v_0 is opposite to that of both u_0 and η_0. For even meridional mode numbers, $|v_0|^2$ will have an extremum at the equator coinciding with the strong but narrow EUC, while $|u_0|^2 + |\eta_0|^2$ will be negligible there. For odd meridional mode numbers the opposite is true. Consequently, the EUC will advect odd modes quite differently than even modes, and a long Rossby wave of a given mode number quite differently than the short Rossby wave of the same mode number.

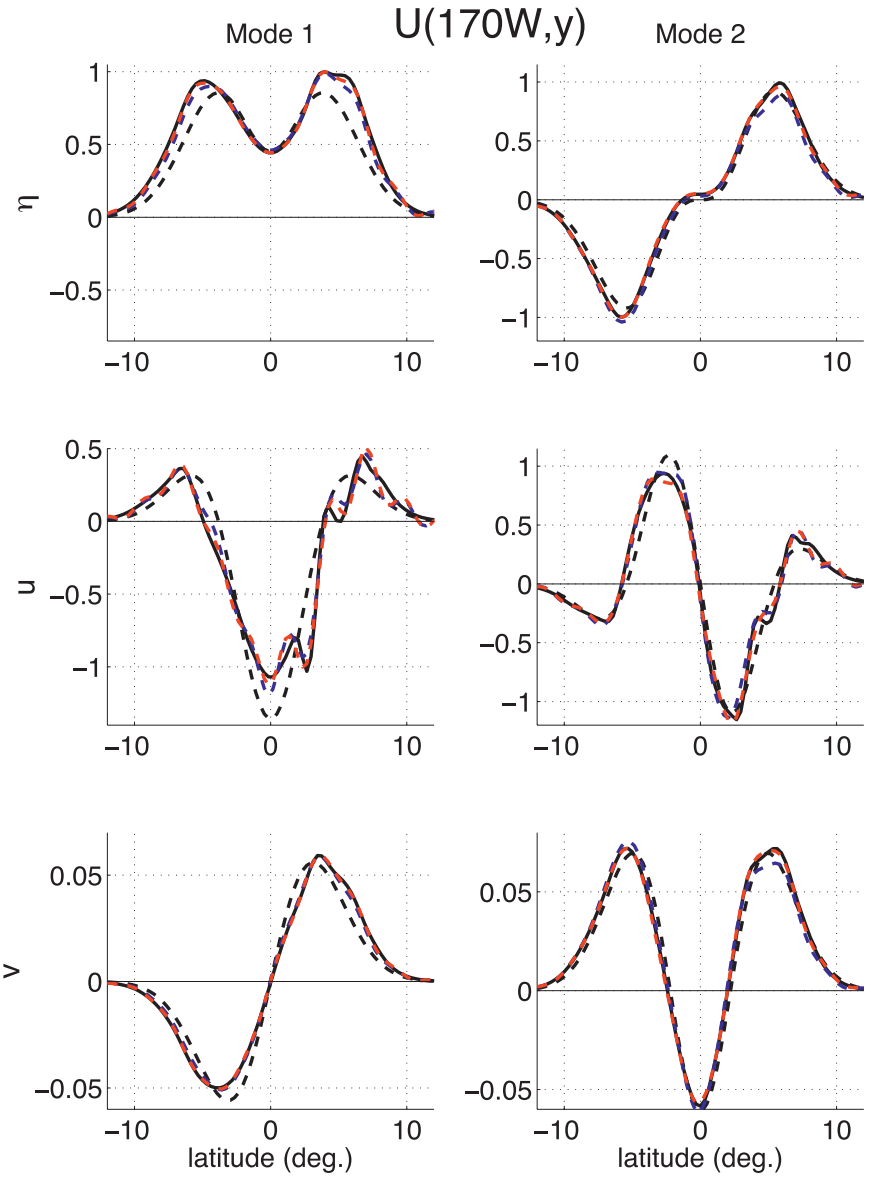

FIG. 7. As in Fig. 6 but for mean currents at 170°W. Thirty Hermite Rossby modes are included in the correction expansions.

The meaning of the second integral in (28) is less clear, and our interpretation of it is a major difference between this and previous work. This is the term consistent with the mechanism, cited by Proehl (1990), involving the advection of background momentum and density fields by the meridional circulation of the wave field. Although Proehl's description fits the form of the integrand, it is not obvious how this mechanism contributes to the wave frequency.

In our efforts to extract more understanding from (28) we are guided by two assumptions. First, we assume that the Rossby wave dynamics are modified but not fundamentally altered by the presence of an $O(\epsilon)$ background current [noting that, for the purpose of understanding (28), we can make the Rossby number ϵ as small as we like]. In particular, we expect the ambient PV gradient to play the same role in the weakly modified Rossby wave dynamics that it does in the rest-state dynamics. Our second assumption is that, under a rearrangement of the mathematical form, (28) should yield terms that are analogous to the Doppler shift term but which reflect the modifications of specific dynamical elements associated with long Rossby waves.

We first note that Ripa (1994) showed that the modal solutions on the rest-state equatorial beta plane can be

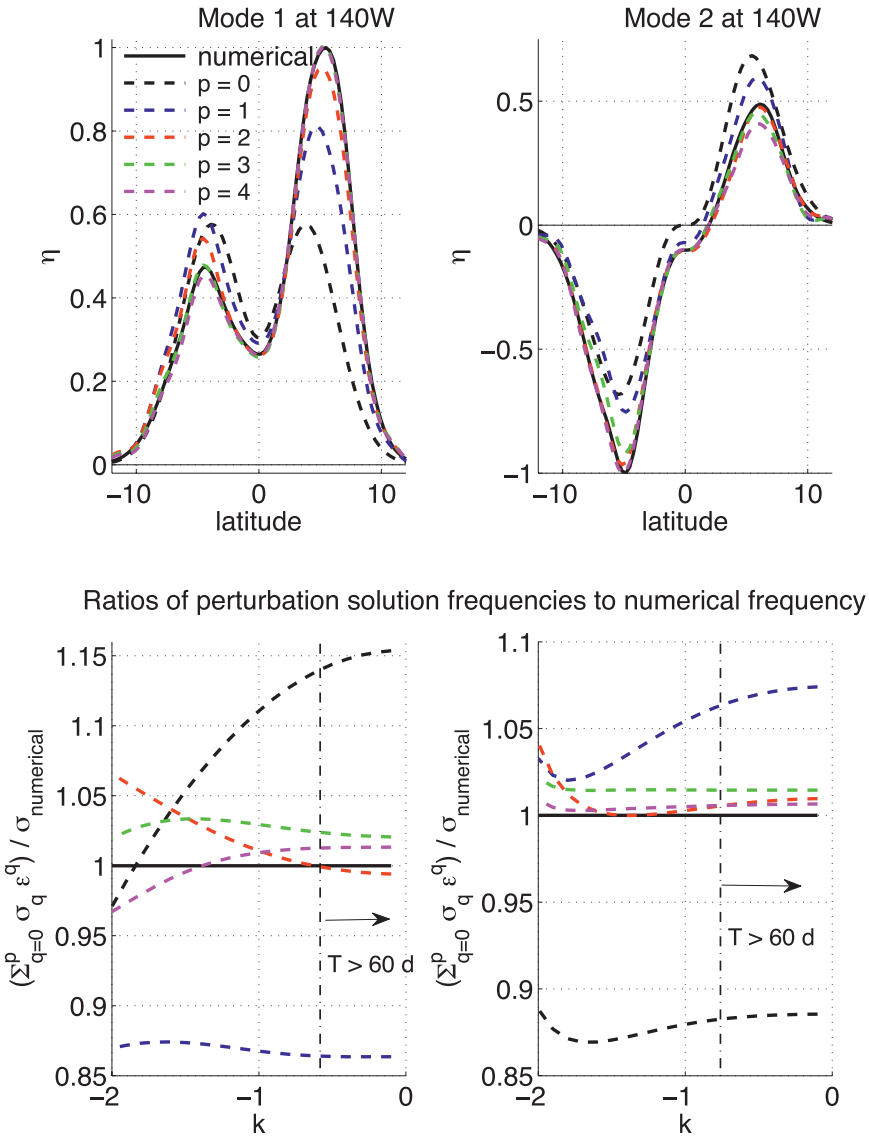

FIG. 8. Convergence of perturbation solutions: numerical and $O(\epsilon^0)$–$O(\epsilon^4)$ solutions for (top) the η eigenfunctions and (bottom) relative frequency curves of (left) mode 1 and (right) mode 2 at 140°W. (bottom) Each curve represents the ratio of a perturbation-solution frequency to the numerical-solution frequency throughout the given wavenumber range. The light, vertical dashed–dotted lines (bottom panels) mark the 60-day long Rossby wave limits shown in Fig. 5. Convergence of the frequency solutions is good within the long Rossby wave range, with the $O(\epsilon^2)$ solution differing from the $O(\epsilon^4)$ solution by at most ≈2%.

reproduced between the turning latitudes by ray-tracing solutions. In the low-frequency limit, the dispersion relation is

$$\sigma_* = \frac{-\beta k_*}{k_*^2 + l_*^2(y_*) + L_d^{-2}(y_*)}, \tag{29}$$

where the asterisk subscripts indicate dimensional variables. In form, (29) is virtually identical to the midlatitude Rossby wave dispersion relation, except that the meridional wavenumber l_* and the inverse-square deformation radius,

$$L_d^{-2} = \frac{f^2(y_*)}{c^2}, \tag{30}$$

are, in this case, functions of latitude ($f = \beta y_*$ is the Coriolis parameter).

Equatorial modes are sometimes thought of as hybrids between Rossby and gravity waves because of the relatively small frequency gap between the Rossby-like and gravity-like solutions and because the Coriolis parameter vanishes on the equator. In the low-frequency limit, however, the solutions of Ripa (1994) demonstrate that locally the dispersion relation depends on β and L_d^{-2} in the same manner as the more familiar midlatitude relations, a correspondence that is not compromised by the vanishing of f on the equator. The low-frequency equatorial modes remain pure vorticity waves. The frequency depends on β, which provides the "restoring force" and does not vanish, and on the effect of the local inverse-square deformation radius L_d^{-2} integrated in some sense between the turning latitudes.

In the presence of a mean current at midlatitudes, the restoring force is modified by the current-induced changes to the ambient PV gradient (e.g., Pedlosky 1987, section 3.18), and we expect this to hold for the equatorial modes. In our nondimensional scheme, the ambient PV is

$$Q = (y - U')/(1 + \delta H) = Q_0 + \epsilon\widehat{\delta Q} + O(\epsilon^2), \tag{31}$$

where

$$Q_0 = y \quad \text{and} \quad \widehat{\delta Q} = -(\widehat{U}' + y\widehat{\delta H}). \tag{32}$$

The $O(\epsilon)$ change to the ambient PV gradient due to the mean currents is then

$$\widehat{\delta Q}' = -\widehat{U}' - (y\widehat{\delta H})'. \tag{33}$$

By analogy with the Doppler shift term, we expect that $O(\epsilon)$ modifications of the phase speed by changes in the ambient PV gradient will be represented by an integral involving the product of $\widehat{\delta Q}'$ and a quadratic form of the $O(1)$ wave field. Because the PV gradient is only important to the extent that wave motions parallel it (i.e., cross the PV contours), the only wave field quadratic that makes sense in this context is v_0^2. The second integral in (28) is reorganized to produce the desired integral using the relations between the $O(1)$ wave components,

$$\begin{pmatrix} u_0^* \\ \eta_0^* \end{pmatrix} = \frac{i}{k^2 - \sigma_0^2}\begin{pmatrix} \sigma_0 y v_0 - k v_0' \\ k y v_0 - \sigma_0 v_0' \end{pmatrix}, \tag{34}$$

and an integration by parts aided by the vanishing of the wave field at infinity. The first part of the integral, for instance, transforms as

$$\begin{aligned} -i\int_{-\infty}^{\infty} \widehat{U}' u_0^* v_0\, dy &= \frac{1}{k^2 - \sigma_0^2}\left[\sigma_0 \int_{-\infty}^{\infty} y\widehat{U}' v_0^2\, dy - k\int_{-\infty}^{\infty} \widehat{U}'\left(\frac{v_0^2}{2}\right)' dy\right] \\ &= \frac{1}{2(k^2 - \sigma_0^2)}\left[\sigma_0 \int_{-\infty}^{\infty} 2y\widehat{U}' v_0^2\, dy + k\int_{-\infty}^{\infty} \widehat{U}'' v_0^2\, dy\right]. \end{aligned} \tag{35}$$

The second part of the integral transforms similarly [using also the governing equation $v_0'' = y^2 v_0 - (\sigma_0^2 - k^2 - k/\sigma_0)v_0$], and we have

$$\begin{aligned} \frac{\sigma_1}{k} = &\int_{-\infty}^{\infty} \widehat{U}(|u_0|^2 + |v_0|^2 + |\eta_0|^2)\, dy \\ &- \int_{-\infty}^{\infty} \widehat{\delta Q}' \frac{|v_0|^2}{2(k^2 - \sigma_0^2)}\, dy - \frac{\sigma_0}{k}\int_{-\infty}^{\infty} \widehat{\delta(Q^2)} \frac{|v_0|^2}{2(k^2 - \sigma_0^2)}\, dy \\ &+ \int_{-\infty}^{\infty} \widehat{\delta H}\left(\eta_0^* u_0 + \frac{\sigma_0}{k}|v_0|^2\right) dy. \end{aligned} \tag{36}$$

In (36), $\widehat{\delta(Q^2)}$ is the $O(\epsilon)$ modification of the squared, ambient PV field,

$$Q^2 = Q_0^2 + \epsilon\widehat{\delta(Q^2)} + O(\epsilon^2) \tag{37}$$

and

$$\widehat{\delta(Q^2)} = -2y(\widehat{U}' + y\widehat{\delta H}). \tag{38}$$

Here Q_0^2 is the nondimensional equivalent of L_d^{-2}, so, in addition to the projection of $\widehat{\delta Q}'$ onto $|v_0|^2$, the reorganization has also produced an integral that plausibly represents the effects of changes to the deformation radius.

The last integral in (36), with $\widehat{\delta H}$ in the integrand, apparently represents the projection of the y-dependent local gravity wave speed onto the features of the wave structure, an interpretation which is supported by a simple thought experiment. Imagine a case where $\widehat{U} = 0$ and $\widehat{\delta H}$ is a constant. This would represent a no-mean-flow case for which we have an analytical solution, but where we have nondimensionalized by the wrong layer thickness and hence the wrong value of c. In the high-frequency gravity wave limit, the terms involving $|v_0|^2$ are negligible and $|\eta_0/u_0| \to 1$. Only $\int \widehat{\delta H}\eta_0^* u_0\, dy$ remains important, and this reduces to $\widehat{\delta H}/2$, which is the proper $O(\epsilon)$ correction to c: $[\gamma H_0]^{1/2} \to [\gamma H_0(1 + \epsilon\widehat{\delta H})]^{1/2}$.

In the low-frequency limit, we contend that the last integral in (36) should be interpreted as part of the modified L_d^{-2} effect, in the same way that c enters into the rest-state dispersion relation (29) only through its effect on L_d^{-2}. Our

TABLE 1. The $O(\epsilon)$ frequency corrections for meridional modes 1 and 2 by $U(140°\text{W}, y)$ and $U(170°\text{W}, y)$. The first column is the meridional-mode number, the second shows the relative frequency change at $O(\epsilon)$, and the following columns give the separate contributions to σ_1 of the individual integrals on the right-hand side of (40). Each column header shows the letter label of the corresponding integral in (40) and the feature of the mean current that appears in the integrand of the term. Note that the $\widehat{\delta Q}'$ term has been separated into its two components: $-\widehat{U}''$ (B1) and $-(y\widehat{\delta H})'$ (B2). In general, the frequency changes are dominated by the advection ($\widehat{U}$) and/or the PV-gradient modification due to the curvature of the mean current ($\widehat{U}''$).

			$\Delta\sigma/\sigma_0$				
Longitude	Mode	$\epsilon\sigma_1/\sigma_0$	(A) $\widehat{U}$	(B1) $-\widehat{U}''$	(B2) $-(y\widehat{\delta H})'$	(C) $\widehat{\delta(Q^2)}$	(D) $\widehat{\delta H}$
140°W	1	−0.25	−0.07	−0.15	−0.02	+0.01	−0.03
	2	+0.21	+0.11	+0.11	−0.01	+0.02	−0.01
170°W	1	−0.22	−0.11	−0.09	−0.01	−0.00	−0.01
	2	+0.044	−0.009	+0.053	−0.004	+0.008	−0.004

analogy between the $\widehat{\delta(Q^2)}$ term and modification of the local deformation radius is probably meaningful, but we do not believe that the third integral in (36) represents the entire deformation radius effect. It is likely, for instance, that the contribution of vortex-stretching dynamics to the long Rossby wave speed would make projections of changes in L_d^{-2} onto $|\eta_0|^2$ relevant. Without better insight into the most efficient representation of this effect, we refrain from further reorganizations. We suggest, however, that in the long Rossby wave limit, the fourth integral in (36), which reflects variability in c through variability in $\widehat{\delta H}$, should be considered together with the third integral as representing the net effect of modifications to the local deformation radius. At any rate, we will see that the first two integrals in (36) dominate phase speed changes in the mean-current systems we are considering, with the last two making only minor contributions.

In the long Rossby wave limit, $\langle|v_0|^2\rangle/\langle|u_0|^2\rangle \ll 1$, $\langle|\eta_0|^2\rangle/\langle|u_0|^2\rangle = 1$, and $|\sigma_0/k| < 1$, so the last term in the last integral in (36) is negligible compared to the second-to-last term. Also in this limit,

$$\frac{1}{2(k^2-\sigma_0^2)} \sim -\frac{\langle|u_0|^2\rangle}{\langle|v_0|^2\rangle}\frac{\sigma_0}{k}(\text{see appendix}), \qquad (39)$$

where the angle brackets indicate integration over the domain. For long Rossby waves, then, (36) can be written as

$$\begin{aligned}\frac{\sigma_1}{k} &= \langle\widehat{U}(|u_0|^2 + |v_0|^2 + |\eta_0|^2)\rangle && \text{(A)}\\ &+ \frac{\sigma_0}{k}\frac{\langle|u_0|^2\rangle\langle\widehat{\delta Q}'|v_0|^2\rangle}{\langle|v_0|^2\rangle} && \text{(B1 + B2)}\\ &+ \left(\frac{\sigma_0}{k}\right)^2\frac{\langle|u_0|^2\rangle\langle\widehat{\delta(Q^2)}|v_0|^2\rangle}{\langle|v_0|^2\rangle} && \text{(C)}\\ &+ \langle\widehat{\delta H}\eta_0^* u_0\rangle && \text{(D)} \qquad (40)\end{aligned}$$

We have labeled the individual integrals A–D for cross-referencing with Table 1. In our subsequent analysis, and in Table 1, the $\widehat{\delta Q}'$ term will be split into its two components: $-\widehat{U}''$ (B1) and $-(y\widehat{\delta H})'$ (B2).

An inspection of Fig. 1 shows that δH is slightly smaller than U and that the meridional scales of the various current features are typically between ½ and 1 equatorial deformation radius. We can thus expect that $|U| \le |U'| \le |U''|$, but we would not expect the various mean-current related terms in (40) to differ by more than perhaps one order of magnitude. Although $\langle|v_0|^2\rangle \ll \langle|u_0|^2\rangle$ in the long-wave limit, the coefficient $\langle|u_0|^2\rangle/\langle|v_0|^2\rangle$, associated with the integrals involving $|v_0|^2$ in (40), makes these integrals potentially of the same order as the advective integral. Indeed, this coefficient keeps the ratio between the PV-related integrals and the advective integral relatively constant throughout the long-wave frequency range, even as the ratio $\langle|u_0|^2\rangle/\langle|v_0|^2\rangle$ changes by many orders of magnitude. For meridional mode m, $\sigma_0/k = -1/(2m+1)$, so for low modes all of the terms in (40) potentially can play a role in the phase speed modification, depending on how the mean-current features project onto the wave functions. We will find that all of the integrals in (40) do make nonnegligible contributions for the current systems under consideration but that the Doppler and $\widehat{\delta Q}'$ integrals tend to be about an order of magnitude larger than the last two integrals.

b. $O(\epsilon)$ solutions at 140° and 170°W

The $O(\epsilon)$ relative frequency corrections ($\epsilon\sigma_1/\sigma_0$) for meridional mode-1 and mode-2 long Rossby waves in the presence of 140° and 170°W mean currents are listed in the second column of Table 1. The remaining columns list the separate contributions to the relative frequency correction made by the individual integrals in (40). Each column header cross-references the integral label from (40) (A–D) and identifies the mean-current feature in the integrand of the relevant term. As noted, the $\widehat{\delta Q}'$

integral has been separated into two components: the effect of $-\widehat{U}''$ (B1) and the effect of $-(y\widehat{\delta H})'$ (B2).

All of the terms make noticeable contributions, but in general the frequency change is dominated by advection ($\widehat{U}$) and the PV-gradient modification due to $\widehat{U}''$, with the latter term accounting for over 40% of the frequency shift in each case. Interestingly, these terms both contribute to the decrease in the mode-1 phase speed and also to the increase in the mode-2 phase speed at 140°W. At 170°W, both terms also contribute to the marked decrease in mode-1 phase speed, but they are both rather small and act counter to each other for mode 2.

Table 1 was compiled for an annual period, but over the range 60 days $< T <$ 3 yr the values represented in Table 1 change by at most a few percent. These small deviations from the values in Table 1 are found at the higher frequencies and are likely due to the $|v_0|^2$ term becoming large enough to influence the advective integral.

c. Graphical analysis of the $O(\epsilon)$ correction

Figures 9–12 present a graphical breakdown of the two dominant terms in Table 1, advection (left column) and modification of the PV gradient by $\widehat{U}''$ (right column), with each figure representing one of the meridional modes at one longitude. The three panels in each column are arranged to illustrate the projection of the mean-current feature onto the important part of the mode-dependent wave structure. The top panel shows the meridional structure of the relevant mean-current feature (U *or* U''), emphasizing the symmetric part [the dynamically important part at $O(\epsilon)$]. The middle panel shows the structure of the relevant $O(1)$ wave component: $(|u_0|^2 + |v_0|^2 + |\eta_0|^2)$ in the case of advection and $|v_0|^2$ in the case of PV-gradient modification. The bottom panel shows the appropriately scaled product of the above two terms, which is the integrand of the relevant term in (40). A positive integral of the curve in the bottom-left panel indicates net advection in the positive x direction, or a slowing of the long Rossby wave's westward phase speed. A positive U'' decreases the strength of the PV gradient and also slows the Rossby wave, so a net positive (negative) area under the curve in the bottom-right panel acts on the phase speed with the same tendency as a net positive (negative) area under the curve in the bottom-left panel. The bottom panels of both columns in all figures are scaled identically to facilitate comparison of the latitude-dependent dynamical effects between modes and between current systems.

Physical insight can now be extracted from the form of the $O(\epsilon)$ frequency correction. The narrow, equatorially centered, eastward EUC dominates the equatorial current system at 140°W (Fig. 9, top left), but the symmetric part of the westward SEC has a maximum amplitude that is roughly 40% that for the EUC (with peaks near 3°S and 3°N) and a total meridional span that is more than twice that of the EUC. Consequently, the net advection could easily be eastward, westward, or negligible, depending on how the meridional distribution of the combined wave-component amplitudes (Fig. 9, middle left) lines up with the currents. The combined amplitudes of mode 1 have a broad meridional span because of the off-equatorial peaks in η_{12} but also a pronounced equatorial peak because of the equatorial maximum of u_{12}. As a result of this peak, the eastward advection by the EUC overpowers the westward advection by the SEC, and the mode-1 westward phase speed is decreased by the advective mechanism. The eastward NECC plays a minor role in changes at the $O(\epsilon)$ level because of its strong asymmetry and particularly at 140°W because of its high latitude.

The rapid change in meridional shear at the core of the EUC dominates the U'' profile, with a negative extremum on the equator (Fig. 9, top right), but the positive curvature associated with the peaks in the SEC (or alternately the flanks of the EUC) remains significant, with peaks near 2°S and 2°N. In fact, because the $O(1)$ meridional velocity of mode 1 has a zero on the equator (middle-right panel), the marked increase in the background PV gradient at the center of the EUC has almost no effect on this mode. Although the increase in the gradient is large, it is confined to a narrow latitudinal strip where wave motions do not parallel the gradient. By contrast, the amplitude of the wave's meridional velocity is close to its maximum at the latitudes where the background PV gradient is decreased near the peaks in the SEC. Consequently, the dominant PV-gradient modification by the mean-current system acts to slow down mode 1, in concert with the advection by the mean current.

In the case of mode 2 (Fig. 10), η_{22} and u_{22} have zeros on the equator, so the strong EUC has very little advective effect on the mode. The off-equatorial maxima in η_{22} and u_{22} coincide quite well with the maxima in the westward SEC, so the advective mechanism acts to increase the westward phase speed of mode 2. The off-equatorial maxima of the meridional velocity of mode 2 (middle-right panel) are somewhat poleward of, and do not overlap well with, the maxima in U'' near the peaks of the SEC. On the other hand, $|v_{22}|$ has a local maximum on the equator where the increase in the background PV gradient associated with the peak of the EUC is at its maximum. Consequently, the dominant PV-gradient-modifying mechanism of the mean currents also acts to increase the phase speed of mode 2.

At 170°W (Figs. 11 and 12) the EUC is somewhat weaker and wider than at 140°W. Its integrated advective

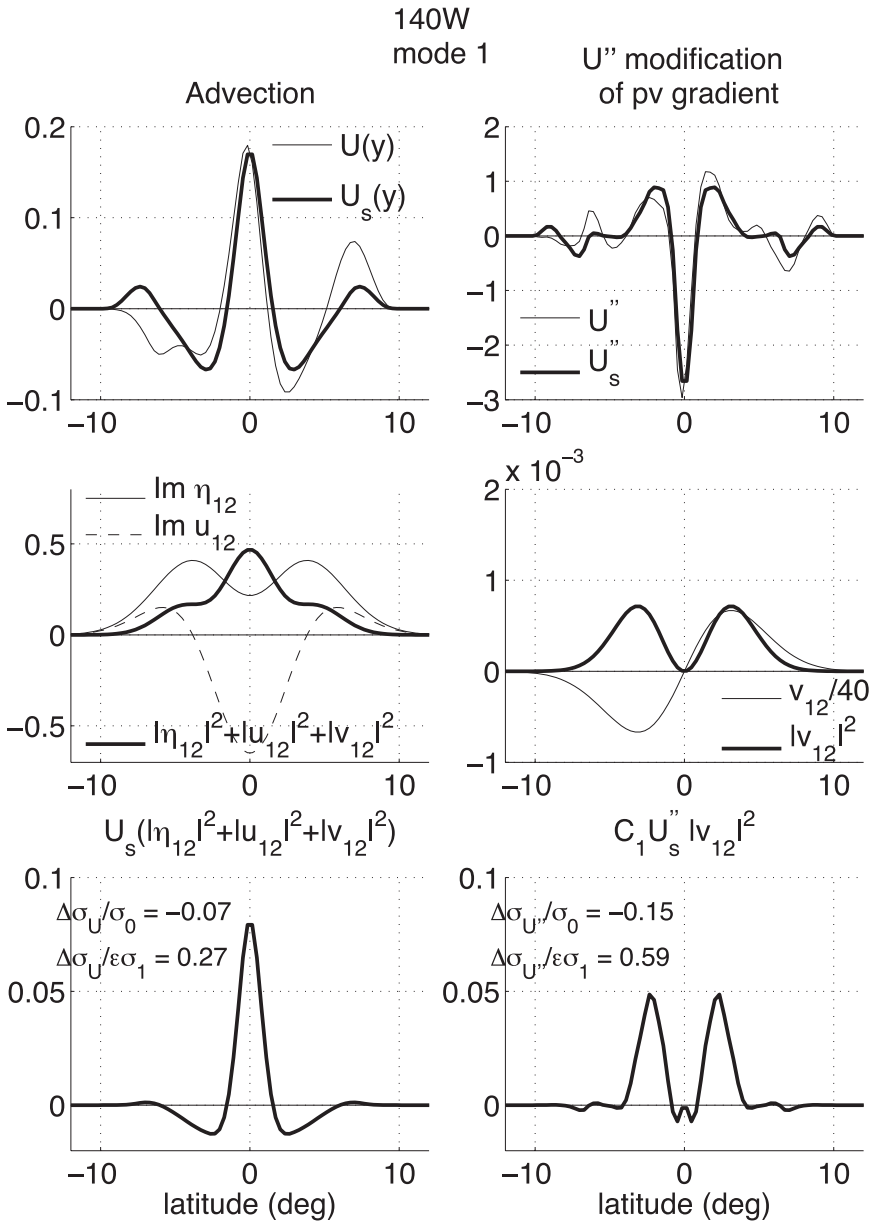

FIG. 9. Effects of (left) advection and (right) U'' on mode-1 phase speed at 140°W: (top) meridional profile of mean-current feature (thin curve) and its symmetric part (thick curve); (middle) squared amplitude of the part of the Hermite wave field affected by the current feature above it; and (bottom) projection of mean-current feature onto relevant wave-field structure (product of thick curves in top and middle rows). Here $C_m = -(\sigma_{m2}/k)\int_{-\infty}^{\infty}|u_{m2}|^2\,dy/\int_{-\infty}^{\infty}|v_{m2}|^2\,dy$, $\Delta\sigma/\sigma_0$ is the relative change in frequency, and $\Delta\sigma/\sigma_1$ is the fractional contribution to the total $O(\epsilon)$ frequency correction.

effect is comparable at the two longitudes, but the associated PV-gradient increase on the equator is significantly weaker at 170°W. The lack of a northern branch to the SEC at 170°W, combined with a more equatorward core of the NECC, significantly decreases the net potential for westward advection compared to 140°W. The small-scale current structure between the EUC and the NECC introduces comparable structure to U_s'' at these latitudes, but the southern branch of the SEC still biases the fluctuations to a net positive U_s'' in the region. Nevertheless, the more equatorward location of the core of the NECC brings a significant negative U_s'' peak closer to the region where it overlaps with the meridional velocity structure of modes 1 and 2.

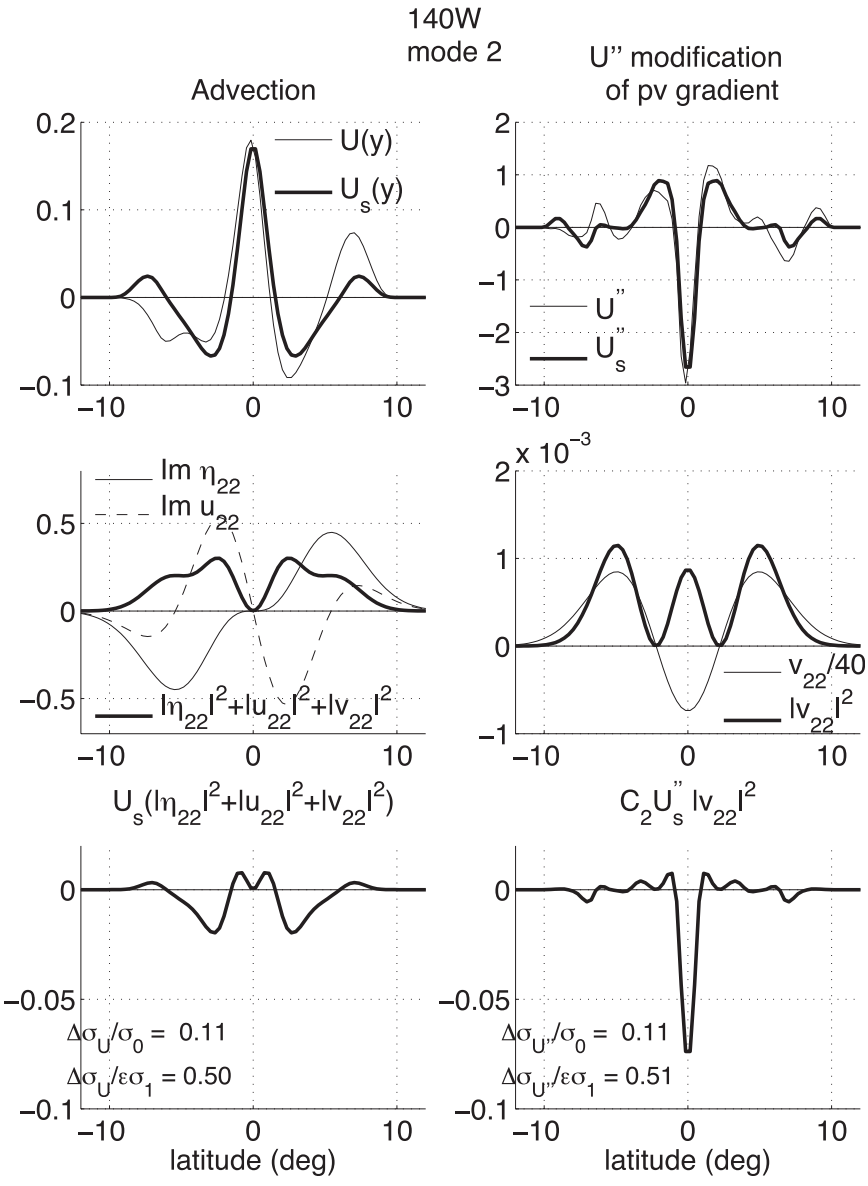

FIG. 10. Effects of (left) advection and (right) U'' on mode-2 phase speed at 140°W, format as in Fig. 9.

The net eastward advective effect of the EUC on mode 1 at 170°W appears to be roughly equivalent to that at 140°W, because the smaller amplitude at 170°W is offset by the increased width. The significantly weaker westward advective effect of the SEC at 170°W, however, results in a larger net eastward advection of mode 1 at 170°W than at 140°W (cf. bottom panels of Figs. 11 and 9). The localized increase in the PV gradient due to the current structure between the EUC and the NECC at 170°W combines with the more equatorward position of the increased PV-gradient contribution from the NECC to partially counter the slowing effect of the decrease in the PV gradient owing to the SEC. Consequently, the net slowing effect on mode 1 associated with U_s'' is somewhat smaller at 170°W than at 140°W. The net effect of the changes in advective potential and PV-gradient modification is that the $O(\epsilon)$ phase speed of mode 1 at 170°W is very similar to that at 140°W, although for slightly different physical reasons.

At 140°W, the narrow EUC had very little overlap with $(|\eta_{22}|^2 + |u_{22}|^2 + |v_{22}|^2)$ and the advection of mode 2 was almost all westward due to the SEC. At 170°W, the wider EUC results in a slightly larger contribution to eastward advection of mode 2 (cf. bottom-left panels of Figs. 12, 10). As noted, the absence of the northern branch of the SEC at 170°W decreases the potential for westward

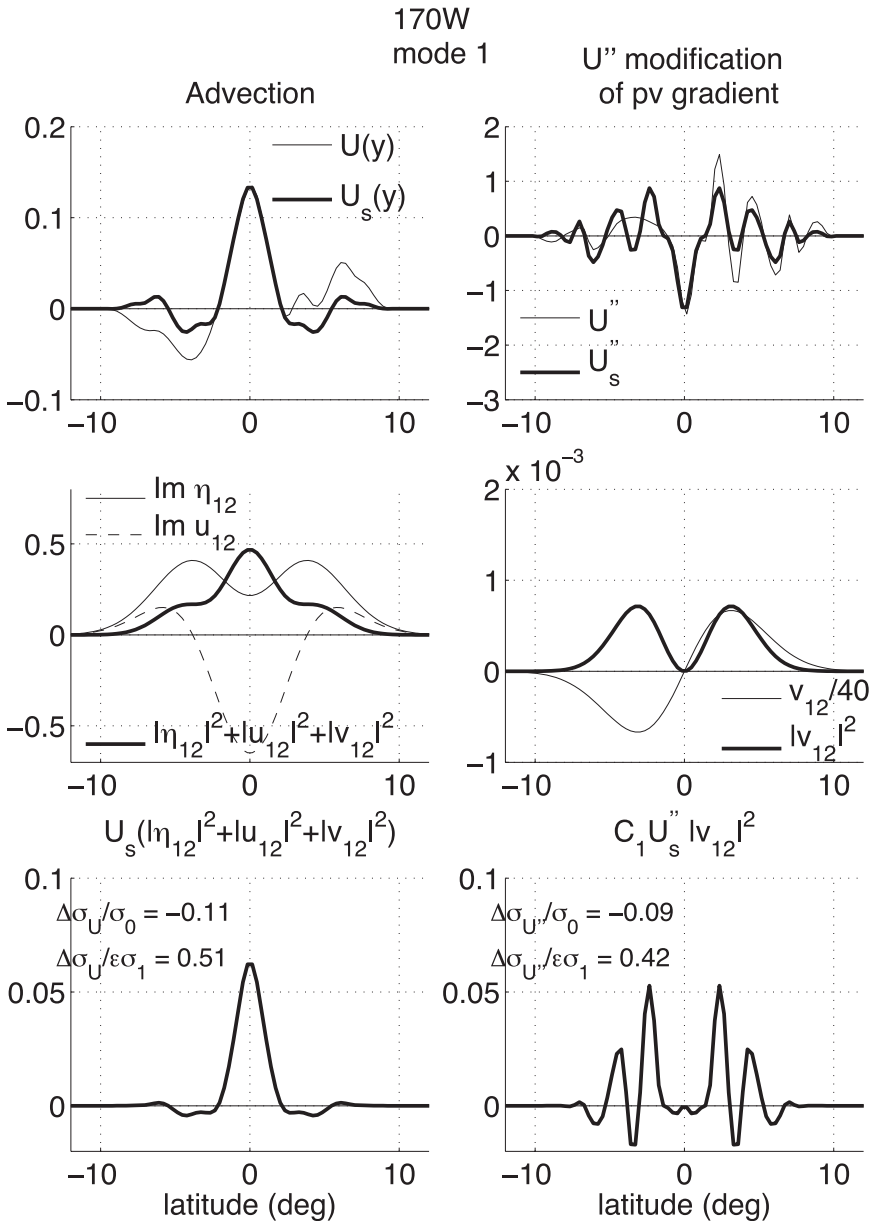

FIG. 11. As in Fig. 10 but on mode-1 phase speed at 170°W.

advection, and the result is a small eastward advection of mode 2 at 170°W. The PV-gradient modification at 170°W still speeds up the westward propagation of mode 2, but the effect is only about half as strong as at 140°W due to the decreased strength and increased width of the EUC at 170°W. In the net, there is a relatively insignificant increase in the phase speed of mode 2 at 170°W.

d. $O(\epsilon^2)$ correction

The analysis of the previous section has provided insight into how the mean currents act upon the Hermite wave vectors to modify the phase speed, and these insights are all that are necessary for a relatively weak current system—for instance, one that has the structure of the 140°W currents but with only ¼ of the full strength. In this case, the changes to the eigenfunctions are minimal, and the $O(\epsilon)$ correction captures the essence of the modification of the dispersion relation (not shown).

When the currents are stronger, however, the wave vectors being acted on by the mean current are significantly different from the Hermite wave vectors, and the $O(\epsilon^2)$ frequency correction becomes important. By changing the order of summation and integration, (25) can be rewritten as

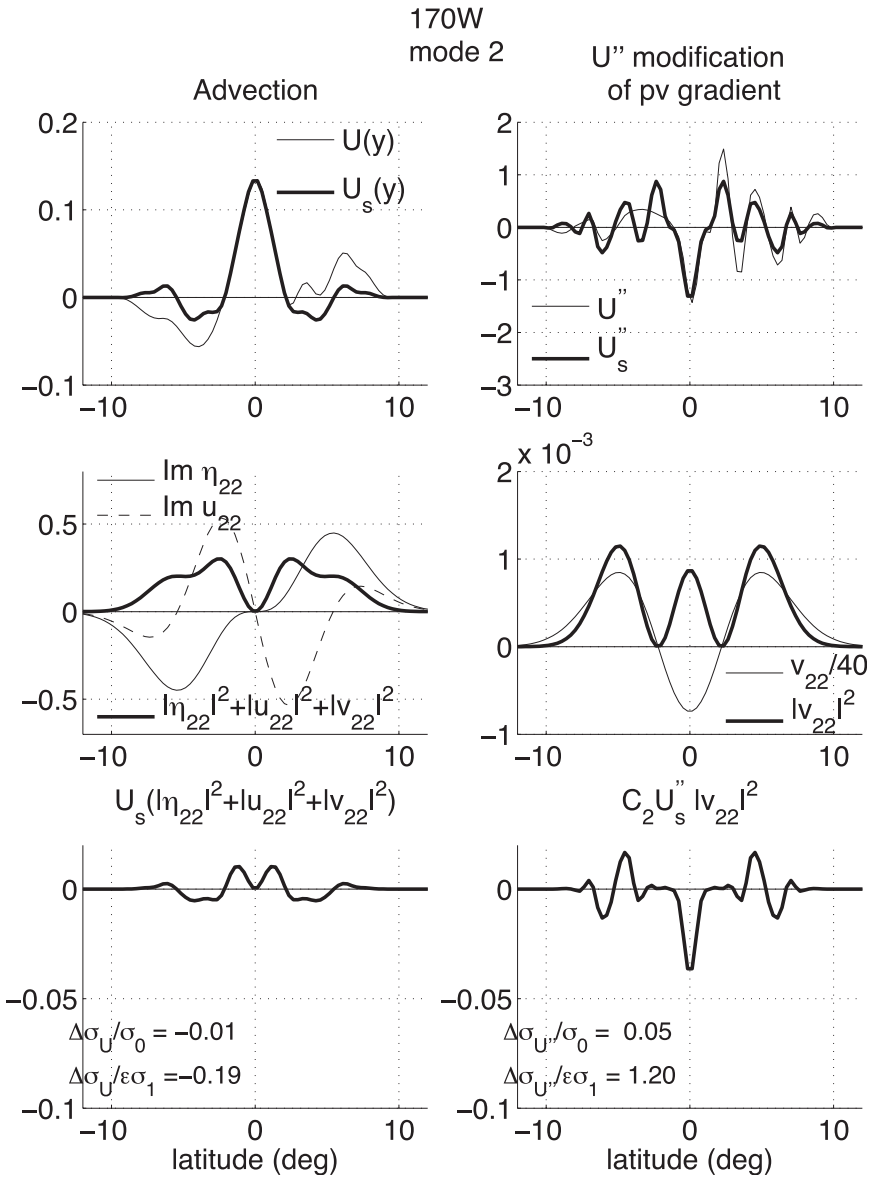

FIG. 12. As in Fig. 10 but on mode-2 phase speed at 170°W.

$$\sigma_2 = -i\int_{-\infty}^{\infty}(u_0 v_0 \eta_0)^* \mathcal{N}_k \begin{pmatrix} u_1 \\ v_1 \\ \eta_1 \end{pmatrix} dy. \tag{41}$$

The $O(\epsilon^2)$ solution can be written as

$$\sigma = \sigma_0 + \epsilon\Delta\sigma, \tag{42}$$

where

$$\Delta\sigma \equiv \sigma_1 + \epsilon\sigma_2 = -i\int_{-\infty}^{\infty}(u_0 v_0 \eta_0)^* \mathcal{N}_k \begin{pmatrix} (u_0 + \epsilon u_1) \\ (v_0 + \epsilon v_1) \\ (\eta_0 + \epsilon \eta_1) \end{pmatrix} dy. \tag{43}$$

Equation (43) demonstrates a similarity between the full frequency correction in the $O(\epsilon^2)$ solution and the $O(\epsilon)$ correction that was analyzed above [cf. (43) with (23)], except that both the $O(1)$ and $O(\epsilon)$ wave-vector solutions are now important.

In general, the analyses of the individual mechanisms are more complex than our analyses at $O(\epsilon)$, but an approximation to the Doppler shift takes a gratifyingly simple form. The form of (43) suggests that we consider a wave vector that is an average of the $O(1)$ and $O(\epsilon)$ solutions:

$$(\overline{u}\,\overline{v}\,\overline{\eta}) = [(u_0 v_0 \eta_0) + (u_0 v_0 \eta_0) + \epsilon(u_1 v_1 \eta_1)]/2. \tag{44}$$

Then we can rewrite (43) as

$$\Delta\sigma = -i\int_{-\infty}^{\infty}(\overline{u}\,\overline{v}\,\overline{\eta})^{*}\mathcal{N}_k\begin{pmatrix}\overline{u}\\ \overline{v}\\ \overline{\eta}\end{pmatrix}dy - \frac{\epsilon}{2}i\int_{-\infty}^{\infty}\left[(u_0v_0\eta_0)^{*}\mathcal{N}_k\begin{pmatrix}u_1\\ v_1\\ \eta_1\end{pmatrix} - (u_1v_1\eta_1)^{*}\mathcal{N}_k\begin{pmatrix}u_0\\ v_0\\ \eta_0\end{pmatrix}\right]dy + O(\epsilon^2). \quad (45)$$

We now consider only the advective part of $\mathcal{N}_k$,

$$\mathcal{N}_{kA} = ik\widehat{U}\mathbf{I} = \mathcal{N}_k - \begin{pmatrix}0 & \hat{U}' & 0\\ 0 & 0 & 0\\ ik\widehat{\delta H'} & \left(\widehat{\delta H'} + \widehat{\delta H}\,\dfrac{d}{dy}\right) & 0\end{pmatrix}, \quad (46)$$

where $\mathbf{I}$ is the identity matrix. When $\mathcal{N}_{kA}$ is substituted for $\mathcal{N}_k$ in (45), the second integral on the rhs vanishes and

$$\frac{\Delta\sigma_A}{k} = \int_{-\infty}^{\infty}\widehat{U}(|\overline{u}|^2 + |\overline{v}|^2 + |\overline{\eta}|^2)\,dy + O(\epsilon^2). \quad (47)$$

To within the accuracy of the solution, the analysis of the full frequency correction due to advection in the $O(\epsilon^2)$ solution is identical to the analysis that we performed at the $O(\epsilon)$ level, except what matters is how the mean current projects onto the average of the rest-state wave vector and the deformed wave vector of the $O(\epsilon)$ solution.

The $O(\epsilon^2)$ frequency correction at 170°W is small compared to σ_0 for both modes (Fig. 5), so in Fig. 13 we illustrate (47) only at 140°W, with the mode-1 (mode-2) advection illustrated in the left (right) column. The format is similar but not identical to that of Figs. 9 and 10. Only U is displayed in the top panel because both symmetric and antisymmetric parts are important in this case. The middle panel displays the important parts of the average wave vector (44), with a subscript indicating the meridional mode number. The thick curve in the bottom panel is again the product of the thick curves in the upper and middle panels and represents the integrand of (47). Only the symmetric part of the integrand contributes to the frequency correction, and this is shown as a thin line for direct comparisons with the integrands shown in the bottom-left panels of Figs. 9 and 10.

Comparing the left panels of Figs. 9 and 13, we see that the important effect on the mode-1 wave vector is the broadening and northward shift of the zonal velocity peak. Because the EUC at 140°W is centered slightly south of the equator, this decreases the eastward advective effect of the EUC while simultaneously increasing the westward advective effect of the SECN. Consequently, the relative slowing of the mode due to advection is reduced from a 7% estimate at $O(\epsilon)$ to 2% at $O(\epsilon^2)$, owing to the distortions in the wave structure. The northward shift of the u and η amplitudes also enhances the advective influence of the NECC but not enough to compensate for the loss of advection by the EUC.

A comparison of the right panels of Fig. 13 with the left panels of Fig. 10 shows that the enhancement and slight equatorward shift of the southern peak of the mode-2 zonal velocity enhances the advective effect of the EUC on this mode. The net advection by the SEC changes little. In total, the relative increase in the westward phase speed of mode 2 due to advection is reduced from an 11% estimate at $O(\epsilon)$ to 7% at $O(\epsilon^2)$.

6. Summary

With numerical solutions of a 1½-layer model of the equatorial Pacific current system, we showed that the effects of mean zonal currents on long equatorial Rossby waves can be somewhat counterintuitive. The effect of the strongest currents (at 140°W) on baroclinic mode 1 is to slow down meridional mode 1 but speed up meridional mode 2. The SSH signal of meridional mode 1 is weakened in the Southern Hemisphere and enhanced in the Northern Hemisphere, but the exact opposite is true for meridional mode 2.

An analysis of a perturbation expansion in the Rossby number ϵ of the mean currents showed that the dominant physical mechanisms affecting the Rossby wave phase speeds in the two current systems considered (140° and 170°W) are advection by the mean currents and modification of the background PV gradient by the curvature in the mean currents, $\widehat{U}''$. As previously shown by Ripa and Marinone (1983) and Proehl (1990), the extent of the advective effect is determined by how well the mean current projects onto the meridional profile of the squared magnitude of the wave vector, $|u|^2 + |v|^2 + |\eta|^2$, which is dominated by $|u|^2 + |\eta|^2$ in the long Rossby wave limit. The PV-gradient effect depends on how well $\widehat{U}''$ projects onto the wave's squared meridional velocity $|v|^2$. The dominance of $\widehat{U}''$ over the interface slope in the PV-gradient modification is no doubt due to the proximity to the equator and the relatively small meridional scale of the currents.

The $O(\epsilon)$ phase-speed solution can be understood in terms of interactions between the mean currents and the structures of the rest-state Hermite wave vectors. This solution is accurate for currents up to about ¼ amplitude of the 140°W currents, and it reproduces the tendency of the phase-speed change even when stronger currents require a higher order solution for accuracy. Opposite

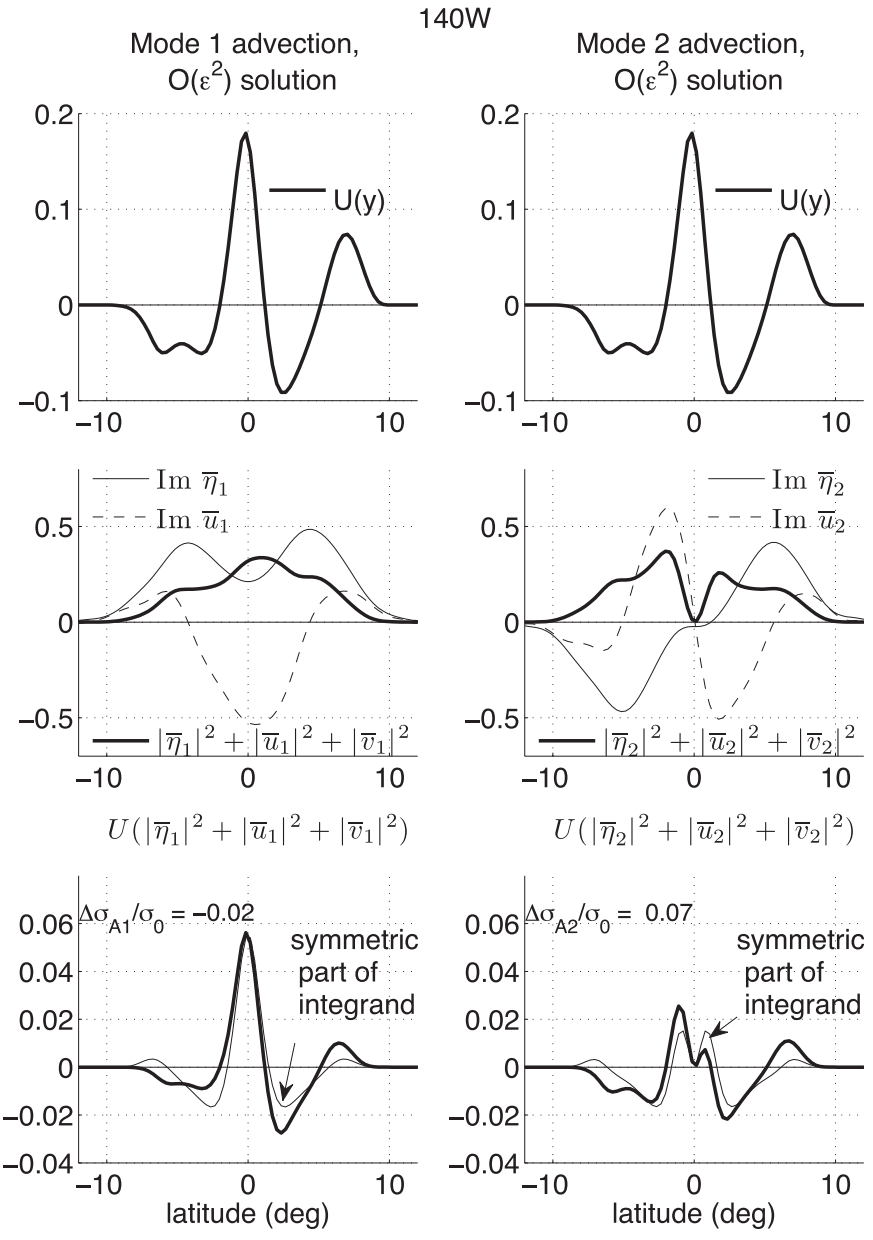

FIG. 13. Advective effects on (left) mode 1 and (right) mode 2 in the $O(\epsilon^2)$ frequency solutions. The format is as in left columns of Figs. 9–12 but (top) the thick curve represents the full U profile (not just the symmetric part), (middle) the important parts of the average wave vectors, defined by (44), are shown with subscripts indicating the meridional-mode number M, and(bottom) the thick curve is the integrand of (47) and $\Delta\sigma_{AM}/\sigma_0$ is the relative change in phase speed by advection in the $O(\epsilon^2)$ solution of mode M.

effects on the phase speeds of modes 1 and 2 are due largely to a coincidence between the meridional scales of the currents and waves and two characteristics of classical equatorial waves: 1) the meridional phases of modes 1 and 2 differ by 90° at the equator and 2) within a single mode the zeros of v are staggered relative to those of u and η. Because mode 1 has a zonal-velocity maximum on the equator, eastward advection by the EUC dominates a weaker westward contribution by the SEC, resulting in net eastward advection of the mode. By contrast, the zonal velocity and pressure of mode 2 have zeros on the equator, whereas the zonal velocity has local extrema near the peaks in the SECS and SECN, thus subjecting this mode to strong westward advection.

The meridional velocity of the Hermite mode 1 has a zero on the equator, so this mode is relatively unaffected by the large increase in the background PV gradient at the core of the EUC. The local extrema of the meridional velocity of mode 1 overlap well with the regions of decreased PV gradient at the peaks of the SECS and SECN, however, contributing to a decreased phase speed. The meridional velocity of mode 2, on the other hand, has a local extremum on the equator where the PV gradient is enhanced and zeros near the peaks of the SECS and SECN where the PV gradient is weakened. The PV-gradient modification thus acts in concert with advection to speed up mode 2.

At 170°W, the general picture for mode 1 is similar to the 140°W scenario (see section 5c for details). For mode 2, however, the weaker PV-gradient enhancement due to a more diffuse EUC combined with weaker advection by a weaker SEC leads to very little change in the dispersion relation.

The above observations depend on the coincidence of wave and current structures, and the results would be quite different for a higher baroclinic mode with a smaller deformation radius. In that case, for instance, the off-equatorial extrema of meridional velocity of mode 1 could conceivably overlap with the region of enhanced PV gradient near the equator so that the advective and PV-gradient effects on mode 1 might act counter to each other. Each mode clearly must be considered separately.

The preceding descriptions are good both qualitatively and quantitatively for a current system up to ~25% of the amplitude of U(140°W) in which wave vectors are changed only moderately from the classical Hermite function wave vectors. At mean-current magnitudes typical of the east-central Pacific, however, distortions of the wave vectors can be significant and can influence the interaction with the mean currents. We have shown that eigenvector distortion (symmetric or antisymmetric) does not affect the phase speed until $O(\epsilon^2)$ and that an antisymmetric part of the current system also cannot affect the phase speed until $O(\epsilon^2)$, which it does through eigenvector distortion at $O(\epsilon)$. Thus, perturbation expansions carried only to $O(\epsilon)$ can miss important parts of the solution. The advective (Doppler shift) effect of the stronger currents on phase speed is qualitatively the same as the $O(\epsilon)$ effect described above, except that we must consider the projection of the mean current onto an average of the Hermite wave vectors and the distorted wave vectors of the $O(\epsilon)$ solution. The interactions of the distorted wave vectors with the changes in the PV field are more complicated, and, although the solutions are given, the details of the PV mechanism at $O(\epsilon^2)$ are not analyzed here.

With the phase speed modification by the stronger currents so dependent on the nature of the wave-vector distortions, a better understanding of the controlling mechanics behind these distortions clearly is needed at this point. Boyd (1978) found that an eastward equatorial jet produced an expansion of the meridional span of the wave vectors while a westward jet produced a contraction (as did Ripa and Marinone 1983), and he attributed these effects to changes in the deformation radius due to U'. To our knowledge, the striking wave-vector asymmetries that appear to be typical of the east-central Pacific have not yet been satisfactorily explained. It is interesting to note that, in the cases we have studied, the wave-vector distortions appear to lessen the impact on the dispersion relations. The $O(\epsilon^2)$ solutions represent an increase in the wave-vector distortions over the $O(\epsilon)$ solutions, but they represent a decrease in the magnitude of the phase-speed shift.

The significant effect that $O(\epsilon)$ changes to the eigenfunctions can have on the phase-speed modification at $O(\epsilon^2)$ raises the possibility that previous perturbation analyses of equatorial waves in mean currents could beneficially be revisited at the higher order. McPhaden and Knox (1979), for instance, analyzed an $O(\epsilon)$ perturbation solution for the Kelvin wave in the presence of an equatorial jet. They showed that short-period (~3 day) Kelvin waves in a 1½-layer model can experience significant eigenfunction distortion at $O(\epsilon)$ by an equatorial jet of similar width and amplitude to our EUC. The distortions included a 10%–20% decrease in the u and η amplitudes on the equator, a broadening of the u and η meridional profiles, and the inclusion of a meridional velocity component with maximum amplitude almost 20% that of the zonal velocity. It is conceivable that these distortions could have a significant effect on the phase speed that was not captured by the $O(\epsilon)$ solution.

Although we have made inroads into a more complete understanding of how zonal currents affect equatorial Rossby modes through modification of the ambient PV field, it is clear that important questions remain even with respect to the dynamics of the 1½-layer model. Extending the insights gained here to a model containing both meridional and vertical shear typical of the equatorial oceans, as well as realistic temporal and zonal variability, is of course the ultimate goal.

Acknowledgments. We thank Jay McCreary for suggesting the perturbation approach, Dennis Moore for guidance and inspiration, and Tom Farrar for many helpful discussions. We also thank Mike McPhaden and two anonymous reviewers for excellent comments that improved the quality of the paper. The work was supported by NASA Grants NNG05GN98G and NNX10AO93G.

APPENDIX

Long-wave approximation of $(k^2 - \sigma_{m2}^2)^{-1}$

In nondimensional variables, the classical expressions for the y dependence of the meridional and zonal velocities of rest-state equatorial Rossby and inertia–gravity waves are (Moore and Philander 1977)

$$v_{mn} = C_{mn}\psi_m(y) \tag{A1}$$

and

$$u_{mn} = C_{mn}\frac{i}{\sqrt{2}}\left(\frac{\sqrt{m+1}}{\sigma_{mn} - k}\psi_{m+1}(y) + \frac{\sqrt{m}}{\sigma_{mn} + k}\psi_{m-1}(y)\right), \tag{A2}$$

where m is the meridional mode number and n denotes one of the three roots of the frequency equation. The Hermite functions ψ_m form an orthonormal basis, so

$$\frac{\langle|u_{mn}|^2\rangle}{\langle|v_{mn}|^2\rangle} = \frac{1}{2}\left[\frac{m+1}{(k-\sigma_{mn})^2} + \frac{m}{(k+\sigma_{mn})^2}\right]. \tag{A3}$$

In the long Rossby wave limit, $\sigma_{m2} \sim -k/(2m+1)$, and (A3) becomes

$$\begin{aligned}\frac{\langle|u_{m2}|^2\rangle}{\langle|v_{m2}|^2\rangle} &\sim \frac{1}{2\sigma_{m2}^2}\left(\frac{1}{4(m+1)} + \frac{1}{4m}\right) = \frac{1}{2}\frac{2m+1}{4m(m+1)\sigma_{m2}^2} \\ &= \frac{1}{2}\frac{(-k/\sigma_{m2})}{(k^2/\sigma_{m2}^2 - 1)\sigma_{m2}^2} = -\frac{k/\sigma_{m2}}{2(k^2 - \sigma_{m2}^2)}.\end{aligned} \tag{A4}$$

Rearranging (A4) we have

$$\frac{1}{2(k^2 - \sigma_{m2}^2)} \sim -\frac{\langle|u_{m2}|^2\rangle}{\langle|v_{m2}|^2\rangle}\frac{\sigma_{m2}}{k}. \tag{A5}$$

REFERENCES

Boyd, J. P., 1978: The effects of latitudinal shear on equatorial waves. Part II: Applications to the atmosphere. *J. Atmos. Sci.,* **35,** 2259–2267.

Chang, P., and S. G. H. Philander, 1989: Rossby wave packets in baroclinic mean currents. *Deep-Sea Res.,* **36,** 17–37.

Chelton, D. B., R. A. deSzoeke, M. G. Schlax, K. El Naggar, and N. Siwertz, 1998: Geographical variability of the first baroclinic Rossby radius of deformation. *J. Phys. Oceanogr.,* **28,** 433–460.

——, M. G. Schlax, J. M. Lyman, and G. C. Johnson, 2003: Equatorially trapped Rossby waves in the presence of meridionally sheared baroclinic flow in the Pacific Ocean. *Prog. Oceanogr.,* **56,** 323–380.

Johnson, G. C., B. M. Sloyan, W. S. Kessler, and K. E. McTaggart, 2002: Direct measurements of upper ocean currents and water properties across the tropical Pacific during the 1990s. *Prog. Oceanogr.,* **52,** 31–61.

Matsuno, T., 1966: Quasi-geostrophic motions in the equatorial area. *J. Meteor. Soc. Japan,* **44,** 25–42.

McPhaden, M. J., and R. A. Knox, 1979: Equatorial Kelvin and inertio-gravity waves in a zonal shear flow. *J. Phys. Oceanogr.,* **9,** 263–277.

——, and P. Ripa, 1990: Wave-mean flow interactions in the equatorial ocean. *Annu. Rev. Fluid Mech.,* **22,** 167–205.

Moore, D. W., and S. G. H. Philander, 1977: Modeling of the tropical ocean circulation. *The Sea,* E. D. Goldberg, Ed., *Marine Modeling,* Vol. 6, John Wiley & Sons 319–361.

Pedlosky, J., 1987: *Geophysical Fluid Dynamics*. 2nd ed. Springer-Verlag, 710 pp.

Philander, S. G. H., 1979: Equatorial waves in the presence of the Equatorial Undercurrent. *J. Phys. Oceanogr.,* **9,** 254–262.

Proehl, J. A., 1990: Equatorial wave–mean flow interaction: The long Rossby waves. *J. Phys. Oceanogr.,* **20,** 274–294.

Ripa, P., 1982: Nonlinear wave–wave interactions in a one-layer reduced-gravity model on the equatorial β plane. *J. Phys. Oceanogr.,* **12,** 97–111.

——, 1994: Horizontal wave propagation in the equatorial waveguide. *J. Fluid Mech.,* **271,** 267–284.

——, and S. G. Marinone, 1983: The effect of zonal currents on equatorial waves. *Hydrodynamics of the Equatorial Ocean,* C. J. C. Nihoul, Ed., Elsevier, 291–317.

Zheng, Q., X.-H. Yan, and C.-R. Ho, 1994: The effects of shear flow on propagation of Rossby waves in the equatorial oceans. *J. Phys. Oceanogr.,* **24,** 1680–1686.